Spring 1-1-2016

Micro-Crawlers in Confined Space: Volume Oscillating Hydrogels

Marti Garriga Font
University of Colorado at Boulder, maga9357@colorado.edu

Micro-Crawlers in Confined Space: Volume Oscillating Hydrogels

by

Marti Garriga Font

B.S./M.S., Universitat Politecnica de Catalunya, 2013

M.S., University of Colorado at Boulder, 2016

A thesis submitted to the

Faculty of the Graduate School of the

University of Colorado in partial fulfillment

of the requirements for the degree of

Master's in Structural Engineering and Structural Mechanics

Department of Civil Engineering

2016

This thesis entitled:
Micro-Crawlers in Confined Space: Volume Oscillating Hydrogels
written by Marti Garriga Font
has been approved for the Department of Civil Engineering

Prof. Franck Vernerey

Prof. Mark P. Stoykovich

Prof. Ronald Y. S. Pak

Date

The final copy of this thesis has been examined by the signatories, and we find that both the content and the form meet acceptable presentation standards of scholarly work in the above mentioned discipline.

Garriga Font, Marti (M.S., SESM)

Micro-Crawlers in Confined Space: Volume Oscillating Hydrogels

Thesis directed by Prof. Franck Vernerey

Recent research has shown that certain polymer hydrogels with simple elongated geometries are capable of moving in a crawling fashion, their motion mechanics inspired by small animals such as earthworms and amoeboids. The focus of this master's thesis is to study the motion capacity of soft matter robots based on polymer hydrogels that undergo periodic inflation and deflation, coupled with symmetry-breaking mechanisms in confined conditions representing a porous channel. A mathematical model in the continuum mechanics frame that evaluates the time-history evolution and motion capabilities of these gels has been developed.

The prime application of these robots is targeted drug delivery; their size, ranging from millimeters to micrometers, and mechanical features which allow for large elastic deformations, make them suitable candidates to carry drugs through porous media like the human body to specific locations, such as tumor cells or damaged tissue, and upon gel degradation release the drug. Targeted drug delivery has two significant advantages compared to current drug application: it allows for customization based on individual patient cellular activity and diminishes side effects. An example of the second advantage is traditional chemotherapy which kills cells that divide rapidly regardless of if they are cancer cells or other cell types that exhibit this behavior in normal circumstances such as bone marrow cells.

One of the main challenges of targeted drug delivery is ensuring that the robot moves successfully from the insertion point to the destination point through human body porous system, hence the motivation for this thesis.

Dedication

This thesis work is dedicated to my family who have been a constant source of support and encouragement, who have always loved me unconditionally and whose good examples have taught me to work hard for the things that I aspire to achieve.

Acknowledgements

I would like to express my sincere gratitude to my advisor Prof. Vernerey for the continuous support of my M.S. studies and related research, for his patience, motivation, and knowledge.

I would also like to thank Prof. Stoykovich for his insights and support of my research.

I thank my fellow labmates for the continuous help and support they gave me specially regarding MATLAB coding.

Contents

Chapter

1 Introduction **1**

1.1 Objectives 1

1.2 Context and applications 1

2 Problem Definition **5**

3 Gel Inflation and deflation **7**

3.1 Introduction 7

3.2 Spherical membrane 7

3.2.1 Solvent flow governing equation 7

3.2.2 Nondimensionalization 9

3.2.3 Swelling ratio 10

3.2.4 Inflating - deflating time characterization 11

3.3 Spherical polymer gel 13

3.3.1 Solvent flow governing equation derivation 13

3.3.2 Nondimensionalization 15

3.4 Characteristic time K_{eq} membrane - gel 16

4 Formulation for a 2D Straight Channel Encapsulating an Elastic Membrane **17**

4.1 Description of the problem 17

4.2 Continuum mechanics formulation 18
4.3 Derivation of the governing equation for the displacement of the membrane in contact with the wall 20
4.4 Derivation of the displacement at deposition time 22
4.5 Solution for basic cases 24
4.5.1 Stick case 24
4.5.2 Free slip case 24

5 Elastic membrane motion in a straight channel: analysis and discussion **25**
5.1 Nondimensionalization 25
5.2 Governing factor μ^* 26
5.3 Directional motion 28

6 Formulation for a 3D Axisymmetric Domain and an Hyperelastic Membrane **31**
6.1 Objectives 31
6.1.1 Kinematics 32
6.1.2 Coordinate system and principal directions 36
6.1.3 Strain and stress 37
6.2 Governing Equations 39
6.2.1 Spherical caps 40
6.2.2 Membrane wall 41
6.2.3 Initial value: displacement at time of deposition "u^D" 45
6.3 Numerical solution to the governing equation 45

7 Membrane Motion Model: Analysis and Discussion **47**
7.1 Convergence 47
7.1.1 Time step convergence 47
7.1.2 Element size convergence 48

7.2 Nondimensionalization 49
7.3 μ^*_{mean} and μ^*_{ratio} 49
7.4 Benchmark problems 50
7.4.1 Low μ^* with straight walls 53
7.4.2 Slip case inclined walls 54
7.5 Mid μ^*: Membrane relaxation 56
7.6 Directional motion 57
7.6.1 μ^*_{ratio} effect on directional motion 58
7.6.2 μ^*_{mean}: rolling versus slippage 59
7.6.3 Confinement effect on directional motion 60
7.6.4 Anchor circle 60

8 Empirical Testing: PNIPAm Gel Motion in Porous Media **61**
8.1 Introduction 61
8.2 Experiment description 61
8.3 Methodology 62
8.3.1 Passive test 63
8.3.2 Active test 64
8.4 Active PNIPAm gel motion 64
8.5 Results 65
8.5.1 Confinement 65
8.6 Ratchet design 66
8.7 Conclusions 68

9 Viscoelastic Slip Coefficient Dependency on Normal Pressure **69**
9.1 Introduction 69
9.2 Shear modulus estimation 69
9.3 Slip coefficient - pressure relationship 70

9.4 Viscoelastic friction and slip model 72

9.5 Implementation of a pressure depending slip coefficient to the numerical model . . . 73

Bibliography **75**

Figures

Figure

1.1 Earthworm Motion 2

1.2 Amoeboid Motion 3

1.3 Leukocyte Motion 3

3.1 Impact of R^* and G^*_{sh} on c 11

3.2 Impact of particle size and stiffness on inflation time 12

3.3 Free inflation - deflation of a membrane time-history 13

4.1 Straight membrane scheme 17

4.2 Interaction wall membrane 19

4.3 Reference current configuration membrane wall 19

4.4 Scheme showing the reference and current configuration at time of deposition and current time of point"a" 20

4.5 Scheme membrane and free body diagram 21

4.6 Scheme material deposition 23

5.1 Graphic C slip vs. displacement 27

5.2 Graphic μ^* vs. strains 27

5.3 3D graphical motion with anisotropy 29

5.4 Center of mass shift over inflation-deflation cycles 30

6.1 Membrane mapping 32
6.2 Spherical cap scheme 34
6.3 Membrane section mapping 35
6.4 Principal directions 36
6.5 Membrane stresses scheme 40

7.1 Time step convergence 48
7.2 Element size convergence 48
7.3 Benchmark high μ^* 52
7.4 Benchmark low μ^* straight walls 54
7.5 Benchmark low μ^* inclined scheme 55
7.6 Benchmark slip inclined 56
7.7 Membrane relaxation and strains 57
7.8 Effect of μ^*_{ratio} on directional motion 58
7.9 Effect of μ^*_{mean} on rolling and slippage 59
7.10 Anchor circle 60

8.1 Channel models schematics 62
8.2 3D printing 62
8.3 Passive test setup 63
8.4 Active test setup 64
8.5 PNIPAm gel inflation-deflation photographs 65
8.6 PNIPAm gel motion photographs 65
8.7 Results confinement 66
8.8 Results gel speed with ratchet in passive test 67
8.9 Results gel speed with ratchet in active test 68

9.1 Compression test photos 70

9.2 confinement relationship with confinement pressure 71

9.3 Slip coefficient pressure dependency 72

9.4 Viscoelastic friction and slip model empirical results 73

Chapter 1

Introduction

1.1 Objectives

The prime objective of this thesis is to support the development of micro-size hydrogels capable of moving in porous medium. Their motion mechanism, inspired by limbless animals such as earthworms, leukocytes and amoeba, is characterized by periodic inflation-deflation coupled with symmetry-breaking mechanisms such as anisotropic friction. We shall break down the objective into three tasks:

(1) Study the inflation-deflation mechanics of polymer gels.

(2) Formulate the motion mechanics of an inflating-deflating spherical hydrogel with anisotropic friction in an axisymmetric channel in a continuum mechanics frame.

(3) Elaborate a MATLAB script that solves numerically the problem described in item (2).

1.2 Context and applications

Soft matter robots motility has been the subject of extensive research. Our focus is on bio-inspired polymer gels of simple elongated geometries capable of moving in confined spaces just like earthworms and amoeboids whose flexible bodies exhibit a continuous interaction with their substrate and have a symmetry-breaking mechanism allowing them to crawl. Earthworm motion is characterized by peristaltic waves (radially symmetrical contraction and relaxation of muscles) traveling throughout their bodies. The wave pushes the earthworm against the substrate, resulting in motion

in the opposite direction of the wave.

Figure 1.1: Scheme of earthworm motion thanks to the peristatic wave. [1]

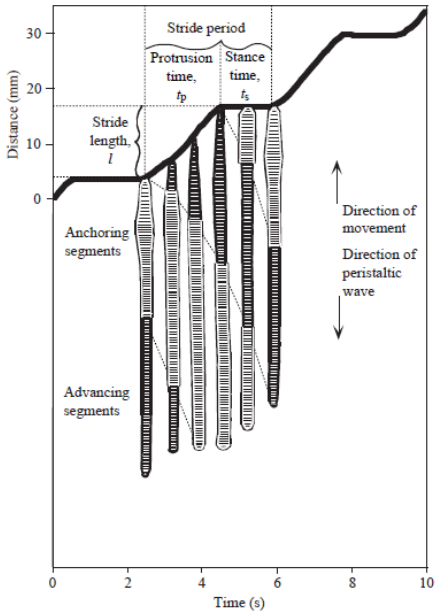

Another example of organisms that move in a crawling fashion are amoeboids. When confined in channels they first react by spreading their bodies across it so that they increase the contact surface. Then, they achieve motion because of alternating protrusions of opposite corners in a zig-zag fashion as shown by Fig.1.2.

Figure 1.2: Experimental results of amoeboid motion. Position of (A) front corners and (B) back corners. [3]

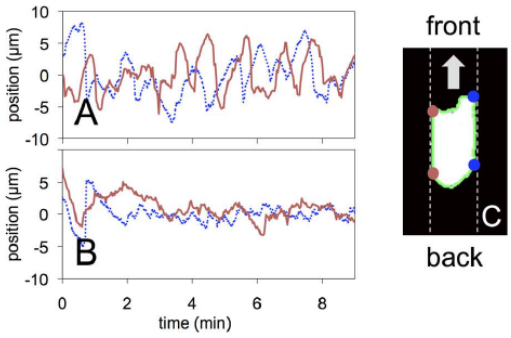

The case of leukocyte (immune system cells, also known as white blood cells) motion is the one that most interests us as its motion mechanics are fundamentally the same as that which we want to achieve for our gels. Leukocyte bodies exhibit large flexibility, they can significantly stretch, contract and adapt their bodies and mode of motion to their environment. When confined, leukocytes achieve motion by protrusion of the leukocyte front, retracting the back of the cell and tuning the adhesion with the substrate.

Figure 1.3: Schematic of leukocyte forward protrusion in confined conditions [7]

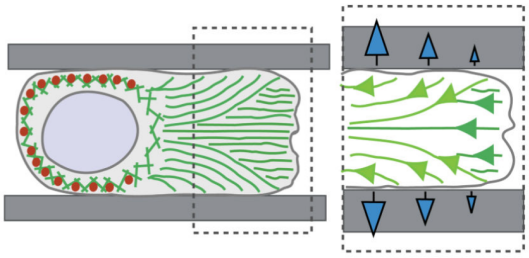

Different polymer gels that exhibit motility have already been synthesized. A well-studied case is the polymer gel composed of a poly(N-isopropylacrylamide) network undergoing the Belousov-Zhabotinsky chemical reaction which show motion in a variety of ways, such as crawling [4] and peristaltic motion [5]. Other examples are photomobile gels [6]. PNIPAm polymer gels have also shown significant potential to move in a crawling fashion. These gels have the same feature in

common: they are capable of periodically inflating and deflating. If this feature is coupled with a symmetry-breaking mechanism, crawling motion can be achieved. This mechanism shall be an anisotropic surface such as a ridged one. Ridged surfaces have already been proved to allow for motion of self-propelled particles [9], which strengthens our novel approach for particle motion. Animals as fish and snake are characterized by a an anisotropic skin, this inspires our approach which consists on an inflating-deflating gel coated with a scales. There is extensive research on the properties of fish skin [10],[11], among them we shall highlight prevents buckling and wrinkling instabilities which is in thin soft matter particles.

The prime application of these robots is targeted drug delivery; their size, ranging from millimeters to micrometers, and mechanical features which allow for large elastic deformations, make them suitable candidates to carry drugs through porous media like the human body to specific locations, such as tumor cells or cartilage tissue, and upon degradation release the drug. It has already shown significant potential in repairing tissue [2] and it has two significant advantages compared to current drug application: it allows for individual customization based on patient cellular activity and diminishes side effects. An example of the second advantage is traditional chemotherapy which kills cells that divide rapidly regardless of if they are cancer cells or other cell types that exhibit this behavior in normal circumstances, such as bone marrow cells which are responsible for production of red blood cells.

One of the main challenges of targeted drug delivery is achieving successful travel of the robot from the insertion point to the destination point through the human body porous system. While periodic inflating-deflating gels have already been synthesized, introducing symmetry-breaking mechanics that would allow those gels to move remains a challenge. Hence, the motivation of this thesis is to help evaluate the motion capabilities of a wide range of gels featuring these characteristics. A subsequent challenge will be to provide the gel with a sense of orientation towards the targeted location, however this is not included in the scope of this thesis.

Chapter 2

Problem Definition

The main challenge of this project is to understand the motion mechanics of a periodically inflating-deflating gel with anisotropic friction confined in a porous medium. Through it we hope we will be able to evaluate its feasibility and help researchers improve their designs to maximize motion. We will first study the mechanics of gel inflation and deflation, as the velocity of the volume cycles and their swelling ratio is directly linked with the directional motion velocity of the gels. Secondly, we will tackle the study of directional motion mechanics of confined gels.

To achieve the second goal we shall establish a model in a continuum mechanics frame that includes all the fundamental physical characteristics of the problem we are studying. We will now enumerate the key assumptions to show the level of complexity and limitations of our model. We will consider a single axisymmetric channel with a smoothly varying radius along a straight axial coordinate which shall represent the porous media inside which the gel will move. The hydrogel is idealized as a droplet encapsulated in an elastic membrane. We chose not to represent the gel as a cross-linked network of elastic strings since it adds a high level of complexity that would not allow for a semi-analytic solution; furthermore, it would difficult discerning how the different features drive the behavior of our problem. The periodic inflation-deflation will be driven through a pressure-controlled experiment; changing the difference in pressure between the inside and the outside of the membrane will implicitly allow us to control its volume. The membrane constitutive equation shall be represented by the hyperelastic model which is appropriate for materials that undergo very large deformations.

Regarding the idealization of the gel as a membrane, note that the volume of gels can be related to the pressure difference (between the inside and outside of the gel) through the polymer-solvent interaction parameter χ. Given the membrane difference in pressure and a specific χ, we can establish a correlation between both systems. Hence, we consider that in this case idealizing the gel as a membrane is a reasonable hypothesis. As the membrane inflates it comes into contact with the channel wall and it slips anisotropically, leading to a shift in the center of mass. The membrane-wall interaction is idealized as a Maxwell model (each point of the membrane in contact with the wall is connected to it through a spring and a dashpot in series). The spring stiffness coefficient is assumed to be very large so that the related displacement is negligible. The slip coefficient is anisotropic which results in our symmetry-breaking mechanism that allows for directional motion. This can be achieved by coating the gel with scales that resemble fish or snake skin. Regarding the angle of contact between wall and membrane, we will assume that the contact is non-wetting and as such, the membrane and wall surface are tangential.

As a starting point, we will idealize the porous medium as a two-dimensional straight channel and a linear elastic model. We will extract valuable information from this case that will help us understand the mechanics of the model we described in the previous paragraph that we will develop after the first simpler one.

Chapter 3

Gel Inflation and deflation

3.1 Introduction

For a gel to move like a leukocyte does in confined conditions, it needs to be capable of periodic swelling and shrinking. In the case of the PNIPAm gel, the gel can be either hydrophilic or hyrophobic depending on its temperature. It is characterized by a lower critical solution temperature (LCST), meaning that with a very small change in temperature it changes abruptly from hydrophilic to hydrophobic or the other way around.
The swelling ratio and the speed of inflation and deflation of the system are linked to the speed the system can achieve. Hence, both aspects shall be studied.

3.2 Spherical membrane

Gels inflation and deflation speed depends on how fast the solvent can flow from the outside of the gel to the inside and the other way around. We will first characterize this feature for a membrane and then for a gel.

3.2.1 Solvent flow governing equation

To estimate the time it takes for the system to swell, we shall formulate the equations of solvent flow through a spherical membrane within the soft matter rheology frame. The flow of solvent through a membrane is given as the difference between the membrane pressure and the osmotic

pressure multiplied by the permeability of the membrane.

$$q = -\kappa_\Gamma([P - \pi]) \tag{3.1}$$

We assume that there is no solute outside the membrane, hence the difference of the osmotic pressure $[\pi]$ can be written as π_{in}.

$$[\pi] = -\frac{k_b T}{v}(\ln(1-\phi) + \chi\phi^2) \tag{3.2}$$

Where ϕ is the volume ratio of solute, χ the solute-solvent interaction parameter, T the temperature, k_b the Boltzman constant and v the volume of a solvent particle. χ is defined by:

$$\chi = \frac{-z \triangle \epsilon}{2k_b T} \tag{3.3}$$

Where z is the coordinator number which represents the number of neighboring cells in the lattice model (typically 8). $\triangle\epsilon$ is the effective interaction between the solute molecules in the solution, if $\triangle\epsilon > 0$ the system tends to phase separate between solute and solvent and so water tends to leave the membrane. If $\triangle\epsilon > 0$ the system tends to mix, and water flows in the membrane. The PNIPAAm gel is characterized by a temperature-dependent effective interaction between solute molecules, $\triangle\epsilon(T)$. Within a small $\triangle T$, $\triangle\epsilon$ changes abruptly, and so the gel volume changes drastically.

Regarding the difference in normal pressure, we shall apply the hyperelastic model to derive it (Equation 6.22). For a stress-free spherical membrane the surface tension can be derived as:

$$\gamma = 2h_0 G_{sh}\left(1 - \frac{1}{\lambda^6}\right) \tag{3.4}$$

Where h_0 is the initial membrane thickness, G_{sh} the shear modulus and λ the radial deformation which is $\lambda = R/R_0$. Remember that the Laplace law reads:

$$[P] = P_{in} - P_{out} = \gamma\frac{2}{R} \tag{3.5}$$

Hence, combining both equations we obtain:

$$[P] = \frac{4h_0 G_{sh}}{R}\left(1 - \frac{1}{\lambda^6}\right) \tag{3.6}$$

We can rewrite this through $R = \lambda R_0$. Note that λ is the strain of the membrane in the in-plane direction which matches with the strain of the radius ($\lambda = C/C_0 = (2\pi R)/(2\pi R_0) = R/R_0$). Hence:

$$[P] = \frac{4h_0 G_{sh}}{R_0}\left(\frac{R_0}{R} - \left(\frac{R_0}{R}\right)^7\right) \tag{3.7}$$

In the case of a membrane confined in a cylindrical channel, the pressure-strain relationship is given by:

$$P_c = \frac{4G_{sh}h_0}{R_{ch}}\left(1 - \frac{1}{\lambda_{cap}^6}\right) \tag{3.8}$$

And so the flow per unit of area of a stress-free membrane:

$$q = -\kappa_\Gamma\left(\frac{4h_0 G_{sh}}{R_0}\left(\frac{R_0}{R} - \left(\frac{R_0}{R}\right)^7\right) + \frac{k_b T}{v}(\ln(1-\phi) + \chi\phi^2)\right) \tag{3.9}$$

For a confined membrane:

$$q = -\kappa_\Gamma\left(\frac{4G_{sh}h_0}{R_{ch}}\left(1 - \frac{1}{\lambda_{cap}^6}\right) + \frac{k_b T}{v}(\ln(1-\phi) + \chi\phi^2)\right) \tag{3.10}$$

The flow through the whole membrane:

$$Q = q4\pi R^2 \tag{3.11}$$

3.2.2 Nondimensionalization

To study what is the impact of each factor in the velocity of inflation and deflation of the membrane, we will proceed to nondimensionalize its change in volume-time ratio.

$$Q = \frac{dV}{dt} = q4\pi R^2 \tag{3.12}$$

We shall nondimensionalize the volume, radius, and time variables.

$$R^* = \frac{R}{R_0} \quad V^* = \frac{V}{V_0} = \frac{R^3}{R_0^3} \quad t^* = \frac{t}{\hat{t}} \tag{3.13}$$

Which yields:

$$\frac{dV^*}{dt^*} = \frac{\hat{t}}{\frac{4}{3}\pi R_0^3} q4\pi R_0^2 R^{*^2} = \hat{t}\frac{3R^{*^2}}{R_0}q \tag{3.14}$$

In order to nondimensionalize q, we will apply $G_{sh} = v_c k_b T$ (where v_c is the number of cross-linked chains per unit volume) and $\phi = \phi_0 \left(\frac{R_0}{R}\right)^3$:

$$q = -\kappa_\Gamma G_{sh} \left(\frac{4t_0}{R_0} \left(\frac{1}{R^*} - \left(\frac{1}{R^*} \right)^7 \right) + \frac{1}{v_c v} \left(\ln \left(1 - \frac{\phi_0}{R^{*3}} \right) + \chi \frac{\phi_0^2}{R^{*6}} \right) \right) \tag{3.15}$$

Then:

$$\frac{dV^*}{dt^*} = \hat{t} \frac{-3R^{*^2} \kappa_\Gamma G_{sh}}{R_0} \left(\frac{4t_0}{R_0} \left(\frac{1}{R^*} - \left(\frac{1}{R^*} \right)^7 \right) + \frac{1}{v_c v} \left(\ln \left(1 - \frac{\phi_0}{R^{*3}} \right) + \chi \frac{\phi_0^2}{R^{*6}} \right) \right) \tag{3.16}$$

Hence we can conclude that the characteristic time $\hat{t}$ is:

$$\hat{t} = \frac{R_0}{\kappa_\Gamma G_{sh}} \tag{3.17}$$

As $\hat{t}$ increases it takes longer for the system to fully inflate and deflate.

For a confined membrane we will consider that the channel radius is proportional to the initial membrane radius and so yields the same characteristic time.

3.2.3 Swelling ratio

To derive the final volume of a membrane, we simply need to impose $q = 0$ in the previously derived solvent flow equation.

$$[P] = [\pi] \tag{3.18}$$

Our concern is to quantify the confinement of the membrane in the channel. Since confinement is related to the area of contact between the channel wall and the membrane, we will show it is directly linked with the capacity of the system to achieve directional motion. We will define the confinement c as:

$$c = \frac{R^s}{R_{ch}} - 1 \tag{3.19}$$

Where R^s is the radius of a stress-free spherical membrane with the same volume as a confined membrane in a channel of radius R_{ch}.

Figure 3.1: Impact of R^* and membrane stiffness G^*_{sh} on the confinement c a membrane can achieve.

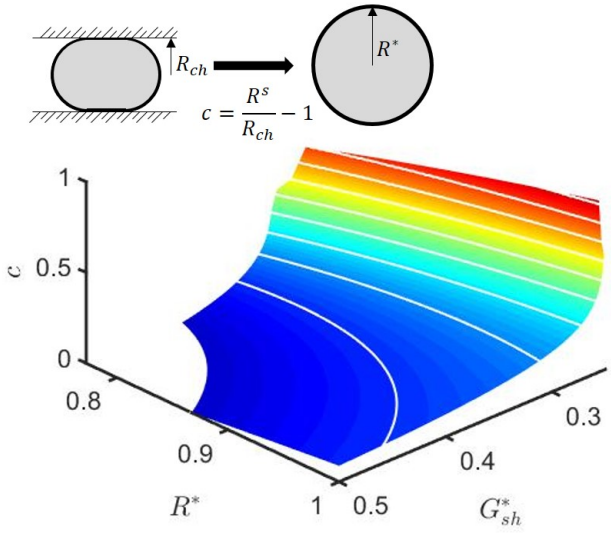

R^* is the ratio between initial membrane radius and channel radius $R^* = R_0/R_{ch}$. The membrane stiffness G_{sh} has been normalized with the membrane pressure $G^*_{sh} = G_{sh}h_0/(P_cR_0)$. Results show that the confinement a membrane can achieve is mainly controlled by its stiffness. As it grows softer, it is able to undergo larger confinements. If the initial position of the membrane is close to the wall, the achieved confinement will also be larger; if the membrane radius is much smaller than the channel it will never come into contact.

3.2.4 Inflating - deflating time characterization

A comprehensive set of numerical tests have been performed to validate $\hat{t}$ and its dependency on the membrane stiffness and the particle size. Note that the results in figure 3.2 are for a constant change in applied pressure, as G_{sh} increases the change in volume will decrease.

Figure 3.2: Impact of particle size and stiffness on a membrane inflation-deflation cycle time for a constant change in applied pressure

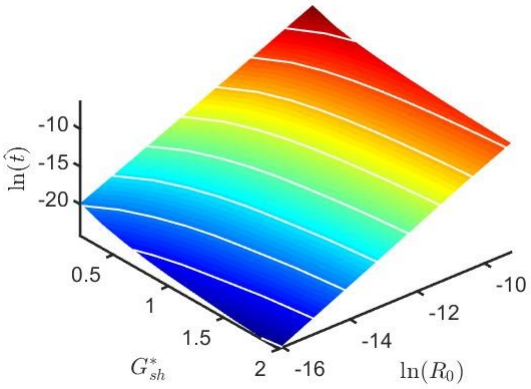

Results are plotted in logarithmic scales for the characteristic time and the particle size. As we can observe from the graphical results, as the membrane grows stiffer and smaller, the time it takes to undergo a full inflation-deflation cycle decreases.

To better understand the mechanics of inflating and deflating the membrane, we shall plot the time history of one cycle.

Figure 3.3: Impact on the flow per unit area (bottom) and on the change in volume (mid) of the change in pressure in a membrane (top), consequence of a step change in the interaction parameter between solvent and solute

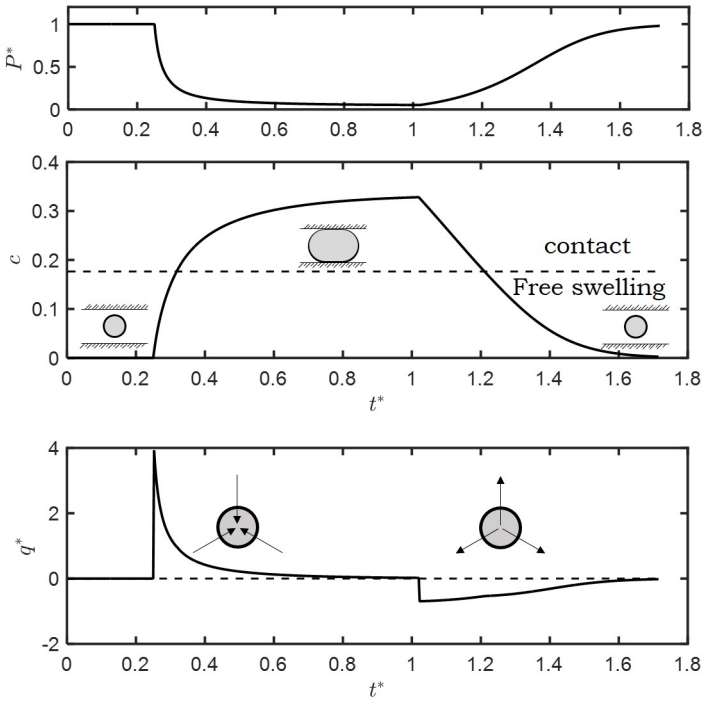

Note that pressure decreases and volume increases because the membrane is modeled with an hyperelastic model which allows for softening. As we can see, the mechanics while confined or in free swelling are fairly similar. Note that the flow per unit surface has been normalized as $q^* = q/(G_{sh}\kappa_\Gamma)$.

3.3 Spherical polymer gel

3.3.1 Solvent flow governing equation derivation

The solvent flow through a polymer gel can be written as:

$$q(r) = -\kappa_\Omega \nabla([P - \pi]) \tag{3.20}$$

Where r is the radius coordinate of the spherical gel and κ_Ω the permeability of the bulk. Note that the flow changes throughout the gel radial coordinate. In the case of a spherical membrane,

the gradient is the derivative with respect to the radial coordinate. The mixing free energy of a polymer gel is:

$$f^{mix} = \frac{k_B T}{v}\left(\frac{\phi}{N}\ln(\phi) + (1-\phi)\ln(1-\phi) + \chi\phi(1-\phi)\right) \tag{3.21}$$

Assuming that the polymer chains are long (high N) the first term vanishes. We can obtain the osmotic pressure through:

$$\pi = -f^{mix} + \phi\frac{\partial f^{mix}}{\partial \phi} \tag{3.22}$$

Which yields the same osmotic pressure as for the membrane:

$$[\pi] = -\frac{k_b T}{v}(\ln(1-\phi) + \chi\phi^2) \tag{3.23}$$

Note that the solute volume ratio ϕ varies according to the radial coordinate, $\phi(r)$.

To derive the pressure for the gel we will first write the deformations gradient in spherical coordinates.

$$F = \begin{pmatrix} \lambda_R & 0 & 0 \\ 0 & \lambda_\theta & 0 \\ 0 & 0 & \lambda_\phi \end{pmatrix} = \begin{pmatrix} \frac{\partial r}{\partial R} & 0 & 0 \\ 0 & \frac{r}{R} & 0 \\ 0 & 0 & \frac{r}{R} \end{pmatrix} \tag{3.24}$$

Where r is the current coordinate and R the reference coordinate of each point of the gel. The elastic stored energy:

$$\psi = \frac{G_{sh}}{2}\left(\left(\frac{\partial r}{\partial R}\right)^2 + 2\frac{r^2}{R^2} - 3\right) \tag{3.25}$$

The nominal stress in radial direction:

$$P_{RR} = \frac{\partial \psi}{\partial \lambda_R} = \frac{\partial \psi}{\partial R}\left(\frac{\partial \lambda_R}{\partial R}\right)^{-1} \tag{3.26}$$

Hence:

$$P_{RR} = G_{sh}\left[\frac{\partial r}{\partial R}\left(\frac{\partial^2 r}{\partial R^2} + 2\frac{r}{R^2}\right) - 2\frac{r^2}{R^3}\right]\left(\frac{\partial^2 r}{\partial R^2}\right)^{-1} \tag{3.27}$$

The reference area:

$$A_0 = 4\pi R^2 \tag{3.28}$$

The current area:

$$A = 4\pi r^2 \tag{3.29}$$

And so we can compute the Cauchy stress in radial direction.

$$\sigma_{RR} = P_{RR}\frac{A_0}{A} = G_{sh}\left[\frac{\partial r}{\partial R}\left(\frac{\partial^2 r}{\partial R^2} + 2\frac{r}{R^2}\right) - 2\frac{r^2}{R^3}\right]\left(\frac{\partial^2 r}{\partial R^2}\right)^{-1}\frac{R^2}{r^2} \tag{3.30}$$

σ_{RR} is the pressure difference we need to plug in the equation for solvent flow through the gel.

$$q(r) = -\kappa_\Omega \frac{\partial}{\partial R}\left(G_{sh}\left[\frac{\partial r}{\partial R}\left(\frac{\partial^2 r}{\partial R^2} + 2\frac{r}{R^2}\right) - 2\frac{r^2}{R^3}\right]\left(\frac{\partial^2 r}{\partial R^2}\right)^{-1}\frac{R^2}{r^2} + \frac{k_b T}{v}(\ln(1-\phi) + \chi\phi^2)\right) \tag{3.31}$$

We can rewrite it as:

$$q(r) = -\kappa_\Omega G_{sh}\frac{\partial}{\partial R}\left(\left[\frac{\partial r}{\partial R}\left(\frac{\partial^2 r}{\partial R^2} + 2\frac{r}{R^2}\right) - 2\frac{r^2}{R^3}\right]\left(\frac{\partial^2 r}{\partial R^2}\right)^{-1}\frac{R^2}{r^2} + \frac{1}{v_c v}(\ln(1-\phi) + \chi\phi^2)\right) \tag{3.32}$$

And the flow through the whole surface:

$$Q(r) = q(r)4\pi r^2 \tag{3.33}$$

3.3.2 Nondimensionalization

To study what is the impact of each factor in the velocity of inflation and deflation of the gel, we will proceed to nondimensionalize its change in volume-time ratio.

$$Q(r) = \frac{dV}{dt} = q(r)4\pi r^2 \tag{3.34}$$

We shall nondimensionalize the volume, radius, and time variables.

$$r^* = \frac{r}{R} \quad V^* = \frac{V}{V_0} = \frac{r^3}{R^3} \quad t^* = \frac{t}{\hat{t}} \tag{3.35}$$

Which yields:

$$\frac{dV^*}{dt^*} = \frac{\hat{t}}{\frac{4}{3}\pi R^3} q 4\pi R^2 r^{*^2} = \hat{t}\frac{3r^{*^2}}{R}q \tag{3.36}$$

Before nondimensionalizing q, we will nondimensionalize the derivatives of r with respect to the original configuration R.

$$\frac{\partial r}{\partial R} = \frac{\partial(r^* R)}{\partial R} = \frac{\partial r^*}{\partial R}R + r^* \tag{3.37}$$

$$\frac{\partial^2 r}{\partial R^2} = \frac{\partial}{\partial R}\left(\frac{\partial r^*}{\partial R}R + r^*\right) = 2\frac{\partial r^*}{\partial R} + \frac{\partial^2 r^*}{\partial R^2}R \tag{3.38}$$

$$q(r) = -\kappa_\Omega G_{sh}\frac{\partial}{\partial R}\Bigg(\left[\left(\frac{\partial r^*}{\partial R}R + r^*\right)\left(2\frac{\partial r^*}{\partial R} + \frac{\partial^2 r^*}{\partial R^2}R + 2\frac{r^*}{R}\right) - 2\frac{r^{*2}}{R}\right]\cdot \\ \cdot\left(2\frac{\partial r^*}{\partial R} + \frac{\partial^2 r^*}{\partial R^2}R\right)^{-1}\frac{1}{r^{*2}} + \frac{1}{v^2}(\ln(1-\phi)+\chi\phi^2)\Bigg) \tag{3.39}$$

Then:

$$\frac{dV^*}{dt^*} = -\hat{t}\frac{3r^{*^2}\kappa_\Omega G_{sh}}{R}\frac{\partial}{\partial R}\Bigg(\left[\left(\frac{\partial r^*}{\partial R}R + r^*\right)\cdot\left(2\frac{\partial r^*}{\partial R} + \frac{\partial^2 r^*}{\partial R^2}R + 2\frac{r^*}{R}\right) - 2\frac{r^{*2}}{R}\right]\cdot \\ \cdot\left(2\frac{\partial r^*}{\partial R} + \frac{\partial^2 r^*}{\partial R^2}R\right)^{-1}\frac{1}{r^{*2}} + \frac{1}{v_c v}(\ln(1-\phi)+\chi\phi^2)\Bigg) \tag{3.40}$$

Hence we can conclude that the characteristic time $\hat{t}$ is:

$$\hat{t} = \frac{R^2}{\kappa_\Omega G_{sh}} \tag{3.41}$$

Note that this is valid at a point in the gel bulk, and to find out how the total volume of the gel varies the flow needs to be integrated throughout the whole bulk.

3.4 Characteristic time K_{eq} membrane - gel

We can relate the characteristic swelling and shrinking time of a membrane and a gel through the factor K_{eq}.

$$K_{eq} = \frac{\hat{t}_{gel}}{\hat{t}_{membrane}} = \frac{\kappa_\Gamma R}{\kappa_\Omega} \tag{3.42}$$

Through this factor we can estimate how fast a gel will inflate and deflate based on the developed model for a membrane. Regarding the swelling ratio, the behavior of the swelling ratio with respect to membrane stiffness and initial confinement R^* is fairly similar given that the mechanics of both systems are very similar.

Chapter 4

Formulation for a 2D Straight Channel Encapsulating an Elastic Membrane

4.1 Description of the problem

In this chapter, our goal is to define a rather simple model that can help us understand the mechanics of the motion of a swelling-deflating droplet covered by an elastic membrane in a porous medium. For that, we will consider two straight parallel walls in a 2D domain confining a membrane with linear elasticity. The mechanism through which the membrane stretches is an increment of the difference in pressure between the droplet and the surrounding media. As the membrane swells, it will come into contact with the wall. Because of the non-symmetry of the slippage between wall and membrane, the membrane's center of mass will move.

Figure 4.1: Membrane swelling scheme, initial configuration (left) and deformed configuration (right)

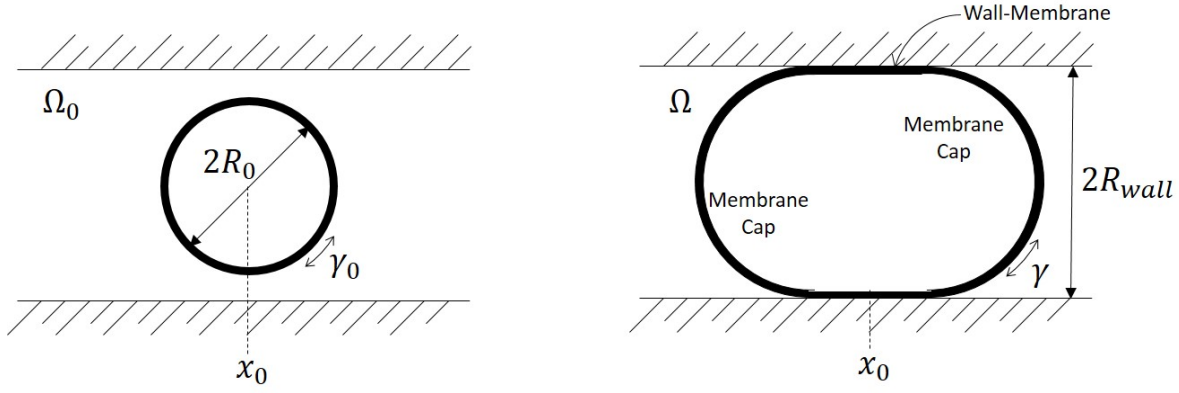

As the membrane swells it will come into contact with the wall and as it carries on swelling the

geometry will change to two circular caps and an expanding rectangle. Another assumption the model includes is that the contact angle between wall and membrane is perfectly hydrophilic, hence equal to 0 degrees. In other words the radius of the caps remain constant equal to half the distance between walls.

4.2 Continuum mechanics formulation

We have chosen to formulate the equations of this system in a continuous mechanics frame. We will separate the domain between the caps and the section of the membrane in contact with the wall.

On the membrane caps we can apply the Laplace's law and the constitutive equation to relate pressure to the deformation of the membrane at the caps. Hence we can easily determine their state

$$\triangle P = \gamma \frac{2}{R} \tag{4.1}$$

$$\gamma = E h_0 \epsilon \tag{4.2}$$

where E is the Young modulus and h_0 is the initial thickness of the membrane. Introducing the constitutive equation into the Laplace's law:

$$\triangle P = E h_0 \epsilon \frac{2}{R} \tag{4.3}$$

The contact forces between wall and membrane will be modeled through a Maxwell model: a spring and a dashpot in series. The spring will account for the friction between membrane and wall due to its roughness. Simultaneously the damper will account for the slippage between wall and membrane. By setting different coefficients on the dashpot according to the direction of motion, the membrane center of mass will shift in one direction, achieving motion.

Figure 4.2: Scheme of the idealized mechanics of surface interaction wall-particle

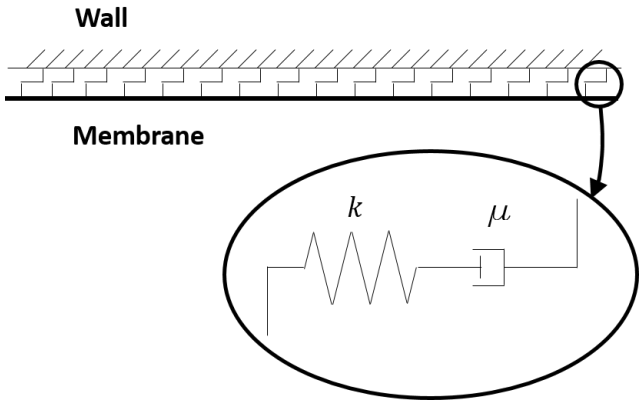

We define X as the unstretched reference coordinates of the membrane. We can write the stretched coordinates of the membrane at any time as a function of the initial state coordinates and the time: $x(X,t)$. Given the current and initial coordinates, the membrane displacement can be written as:

$$u(X,t) = x(X,t) - X \tag{4.4}$$

This can be depicted through the following scheme:

Figure 4.3: Scheme with the reference coordinates X (top) and current x (bottom) at the membrane-wall contact

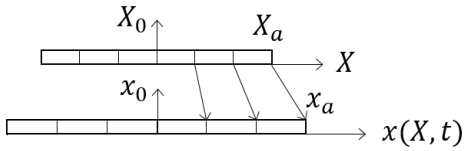

A quantity in which we are particularly interested is the membrane-wall displacement, which we can define as the difference between the current coordinates of the membrane and the coordinates of the membrane at the time at which it comes into contact with the wall. We call this time instant "deposition time". This quantity can be formally written as:

$$u^{MW}(X,t) = x(X,t) - x(X,t_d) \tag{4.5}$$

To better understand the physical meaning of $x(X,t_d)$ we can look at the next scheme:

Figure 4.4: Scheme showing the reference and current configuration at time of deposition and current time of point"a"

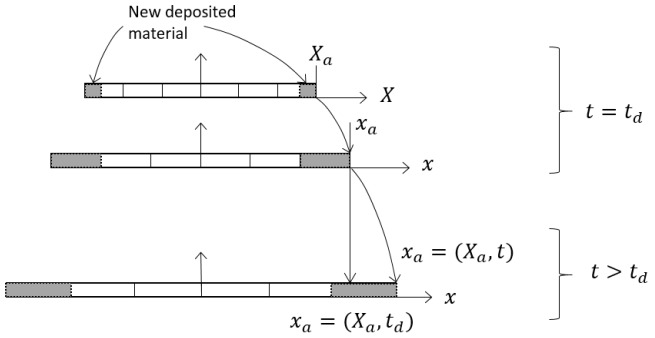

Given that the interaction between the wall and membrane is governed by the Maxwell model previously stated, once the membrane gets into contact with the wall it will start experiencing slip deformation. The anisotropy of this slippage will determine the motion of the body. Hence it is of our interest to define the membrane-wall displacement which we will write as:

$$u^{MW}(X,t) = x(X,t) - X + X - x(X,t_d) = u(X,t) - u^d(X,t_d) \tag{4.6}$$

Where:

$$u^d(X,t_d) = x(X,t_d) - X \tag{4.7}$$

u^d is the displacement at time of deposition, in other words, the displacement of each point of the membrane at the time it comes into contact with the wall. The membrane-wall displacement, u^{MW}, is directly related with the frictional forces between wall and membrane through application of the Maxwell model:

$$F_{fr}(X,t) = k u_e^{MW}(X,t) = \mu \dot{u}_s^{MW}(X,t) \tag{4.8}$$

4.3 Derivation of the governing equation for the displacement of the membrane in contact with the wall

Consider a free body diagram on a segment of the membrane segment in contact with the wall.

Figure 4.5: Scheme of reference membrane configuration (a), current configuration (b) and free body diagram of a section of a membrane in contact with the wall (c)

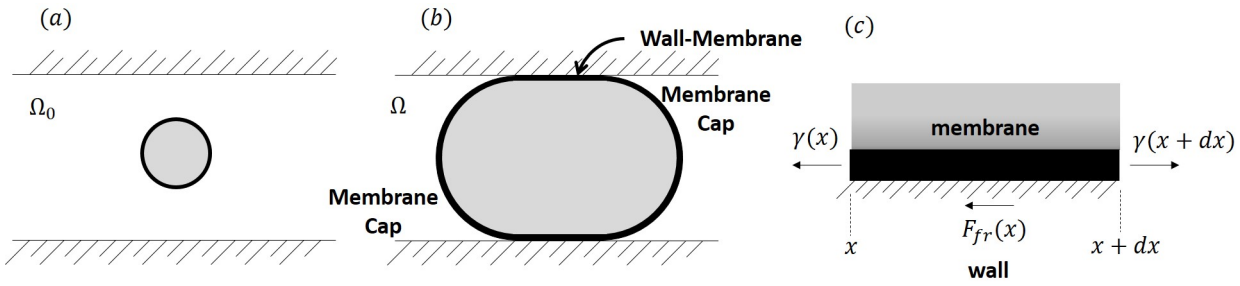

We shall establish equilibrium of forces, noting that we are assuming the problem to be quasi-static so that the acceleration of the system is considered to be negligible; hence:

$$\sum F_x = 0 \tag{4.9}$$

Which yields:

$$\frac{\partial \gamma}{\partial x} - F_{fr} = 0 \tag{4.10}$$

Where γ stands for the surface tension of the membrane and F_{fr} for the frictional forces. We will assume that the the displacements are small enough so that we can write $\frac{\partial \gamma}{\partial x} \approx \frac{\partial \gamma}{\partial X}$. Resulting in:

$$\frac{\partial \gamma}{\partial X} - F_{fr} = 0 \tag{4.11}$$

Recall the linear stress-strain constitutive model:

$$\gamma(X,t) = Eh_0 \frac{\partial u}{\partial X} \tag{4.12}$$

Plugging it in the derived equation:

$$Eh_0 \frac{\partial^2 u}{\partial X^2} - F_{fr} = 0 \tag{4.13}$$

Assuming that the velocity of the elastic displacement and of the displacement at deposition is negligible compared to the slip velocity between wall and membrane:

$$\dot{u} = \dot{u}^{MW} + \dot{u}^{d} \approx \dot{u}^{MW} \tag{4.14}$$

And:

$$\dot{u}^{MW} = \dot{u}_e^{MW} + \dot{u}_s^{MW} \approx \dot{u}_s^{MW} \tag{4.15}$$

Hence:

$$F_{fr} = \mu \dot{u}_s^{MW} = \mu \dot{u} \tag{4.16}$$

We can rewrite the governing equation as:

$$Eh_0 \frac{\partial^2 u}{\partial X^2} - \mu \dot{u} = 0 \tag{4.17}$$

Which we can rewrite as:

$$\frac{\partial u}{\partial t} = \frac{Eh_0}{\mu} \frac{\partial^2 u}{\partial X^2} \tag{4.18}$$

The derived governing equation is equivalent to the partial differential equation for the classic heat transfer problem in the 1D case. We shall determine the proper initial and boundary conditions for the derived partial differential equation. Given the pressure, we know the deformation at the caps of the membrane through Laplace's law and the constitutive stress-strain relationship. Hence, the boundary conditions is set to enforce the continuity of deformations at both ends of the contact length.

$$\frac{\partial u}{\partial X}(X_{end,+}, t) = \epsilon_{cap} \qquad \frac{\partial u}{\partial X}(X_{end,-}, t) = \epsilon_{cap} \tag{4.19}$$

We solved this problem using a pressure step-wise scheme. Consequently, for a given step "i" the initial condition is set as:

$$u(X, t_i) = u^{MW}(X, t_{i-1}) + u^d(X, t_i) \tag{4.20}$$

4.4 Derivation of the displacement at deposition time

Before solving the governing equation we need to derive an expression for the displacement at deposition time $u(X, t_d)$. We will do so by utilizing the Taylor's expansion. For that we will consider a piece of membrane as depicted by the following figure.

Figure 4.6: Scheme of deposition of material at reference and current configuration

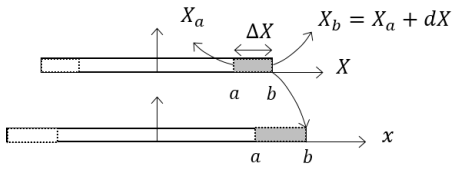

Given that we are solving in a pressure step-wise scheme let's assume that in a given step $\triangle X$ is the newly deposited membrane material into the wall. From the previous step we know the displacement at deposition from all the points that already were deposited and in particular of the point "a", $u^d(X_a)$. We shall derive the displacement at contact time throughout $\triangle X$.

Recall the definition of $u^d(X,t)$:

$$u^d(X_a) = x_a(t_d) - X_a \tag{4.21}$$

$$u^d(X_b) = x_b(t_d) - X_b \tag{4.22}$$

As previously stated, we assumed an elastic constitutive model for the membrane deformation. Through it we know the deformation at point "a" which remains constant once the membrane touches the wall in the non-slip case. We also know the deformation at the end of the deposited amount of material, point "b", which is the deformation of the cap, obtained through Laplace's law.

Given that the coordinate in the unstretched configuration X_b is known, we solely need to derive $x_b(t_d)$ which we will obtain through Taylor series:

$$x_b(t_d) = x_a(t_d) + \left[\frac{\partial x}{\partial X}\right] dX + \frac{1}{2}\left[\frac{\partial^2 x}{\partial X^2}\right] dX^2 + H.O.T. \tag{4.23}$$

We will ignore the higher order terms since we assumed linear deformations. As such, we will substitute the derivatives using the definition of deformation $\epsilon = \partial u/\partial X$:

$$\epsilon = \frac{\partial u}{\partial X} = \frac{\partial(x(X,t) - X)}{\partial X} = \frac{\partial x}{\partial X} - 1 \qquad \frac{\partial x}{\partial X} = \epsilon + 1 \tag{4.24}$$

Plugging it in Equation 18:

$$x_b(t_d) = x_a(t_d) + [1+\epsilon]\, dX + \frac{1}{2}\left[\frac{\partial \epsilon}{\partial X}\right] dX^2 + H.O.T. \tag{4.25}$$

Given that the strain is linear, we can write:

$$\epsilon(X) = \epsilon(X_a) + \frac{\partial \epsilon}{\partial X}(X - X_a) \tag{4.26}$$

We also know the deformation at X_b which is the same as the deformation of the cap as previously stated, and we will use it to find an estimate for $\frac{\partial \epsilon}{\partial X}$:

$$\epsilon(X + \triangle X) = \epsilon(X_b) \tag{4.27}$$

Which is also equal:

$$\epsilon(X + \triangle X) = \epsilon(X_a) + \frac{\partial \epsilon}{\partial X}(X_a) \triangle X \tag{4.28}$$

Hence:

$$\frac{\partial \epsilon}{\partial X} = \frac{\epsilon(X_b) - \epsilon(X_a)}{\triangle X} \tag{4.29}$$

And so we can find $x_b(t_d)$ by plugging the deformation and its derivative into the Taylor's expansion stated.

$$x_b(t_d) = x_a(t_d) + \epsilon(X_b)dX + \frac{1}{2}\frac{(\epsilon(X_b) - \epsilon(X_a))}{\triangle X}dX^2 \tag{4.30}$$

4.5 Solution for basic cases

4.5.1 Stick case

In the case that there is no slip we have that u^{MW} is zero at all points, hence $u(X,t) = u^d$ which is known.

4.5.2 Free slip case

In the case where the whole membrane can slip freely, the equilibrium condition will be given by a uniform deformation all through the membrane. Given that the deformation is known at the caps through Laplace's law, we can derive the displacement through the entire membrane.

Chapter 5

Elastic membrane motion in a straight channel: analysis and discussion

In this chapter we will analyze and discuss the results of the model defined in the previous chapter.

5.1 Nondimensionalization

To assess the relative importance of the terms that govern the system and facilitate the scale-up of the obtained results we will transform our variables so that we can work with dimensionless parameters. We will normalize the governing equations:

$$P = \epsilon_c \frac{2Eh_0}{R} \tag{5.1}$$

$$\frac{\partial u}{\partial t} = \frac{Eh_0}{\mu} \frac{\partial^2 u}{\partial X^2} \tag{5.2}$$

For that, we will establish the following dimensionless variables and numbers:

$$t^* = \frac{\dot{P}R}{Eh_0} t \quad u^* = \frac{u}{R} \quad X^* = \frac{X}{R} \quad P^* = \frac{R}{Eh_0} P \tag{5.3}$$

We shall show that t^* is dimensionless:

$$[t^*] = \left[\frac{\dot{P}R}{Eh_0} t \right] = \frac{F}{L^2 T} L \frac{L}{F} T = [-] \tag{5.4}$$

Note that the dimensions of the slip coefficient are given by:

$$[\mu] = \left[\frac{F_{fr}}{\dot{u}} \right] = \frac{F}{L^2} \frac{T}{L} = \frac{FT}{L^3} \tag{5.5}$$

The frictional forces dimensions are given by the previously stated equation:

$$\frac{\partial \gamma}{\partial X} = F_{fr} \qquad \left[\frac{\partial \gamma}{\partial X}\right] = \frac{F}{L^2} \tag{5.6}$$

Introducing the dimensionless variables into the Laplace's law yields:

$$\epsilon = \frac{R}{2Eh_0}\frac{Eh_0}{R}P^* \tag{5.7}$$

Which can be rewritten as:

$$\epsilon = \frac{P^*}{2} \tag{5.8}$$

And doing the same in the governing equation for the displacement of the membrane in contact with the wall:

$$\frac{\dot{P}R}{Eh_0}R\frac{\partial u^*}{\partial t^*} = \frac{Eh_0}{\mu}\frac{R}{R^2}\frac{\partial^2 u^*}{\partial X^{*2}} \tag{5.9}$$

Which can be rewritten as:

$$\frac{\mu \dot{P} R^3}{(Eh_0)^2}\frac{\partial u^*}{\partial t^*} = \frac{\partial^2 u^*}{\partial X^{*2}} \tag{5.10}$$

The derived non-dimensional factor controls the behavior of the system. If it increases, the amount of slippage the membrane undergoes decreases. We will simplify this factor and call it μ^*:

$$\mu^* = \frac{\dot{P}\mu R^3}{(Eh_0)^2} \tag{5.11}$$

Regarding the output variables:

$$u^* = \frac{u}{R} = \frac{u^{MW}}{R} + \frac{v}{R} = u^{MW^*} + v^* \tag{5.12}$$

5.2 Governing factor μ^*

An exhaustive number of computational tests have validated the consistency of the derived slip driving coefficient μ^*. Results are summarized in figures 5.1 and 5.2.

Figure 5.1: Results for an inflating membrane with different μ^*: pressure time history (top), displacement at the end of the contact length (middle) and velocity (bottom graphic).

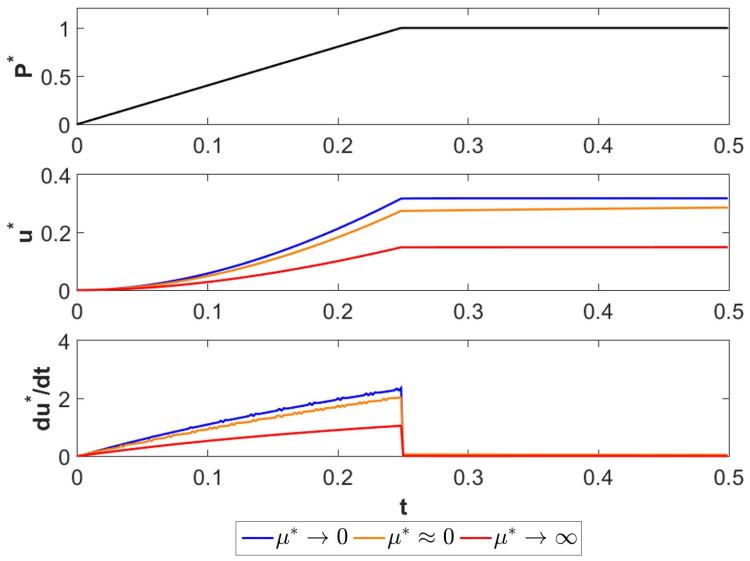

Figure 5.2: Impact of different μ^* on the strains of an inflating membrane

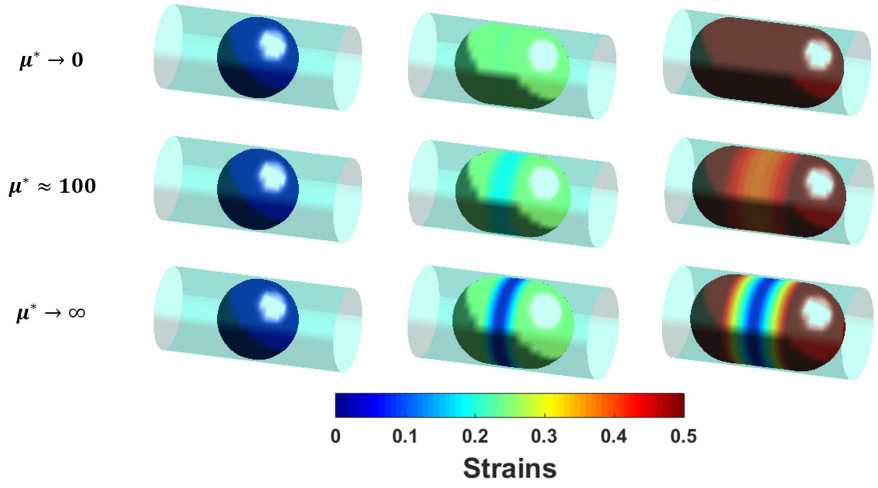

In the case that the membrane does not slip on the wall, related to a high μ^*, the displacement of the membrane is a consequence exclusively of the stretching of the caps that, over time, leads to increasingly deformed material being deposited on the walls. Once a membrane portion deposits on the wall, it cannot stretch further and, as a result, the strain profile of the membrane over the wall is linear, matching the strain of the cap at both ends and the strain at the time the membrane first comes into contact with the wall at the center. We can infer that the frictional forces, equal

to the first space derivative of the strain multiplied by the Young modulus (Equation 4.13), have a constant absolute value across the contact length with a sharp corner at the center and different sign at each side, accounting for the direction of the force.

In the event that the membrane can slip freely on the wall (low μ^*), the nondimensionalized displacement is a consequence of both the slippage and the deposition of stretched material from the caps on the walls. As we can observe, the total displacement is nearly twice as the one in the non-slip case (Figure 5.1). The strain of the membrane in contact with the wall matches at any time the strain of the caps (bottom of Figure 5.2). Consequently, the frictional forces are nil throughout the membrane-wall contact.

In the partial slip case (mid μ^*), the membrane in contact with the wall stretches over time; however, it does not match the deformation at the caps at all times. The shape of the deformation is somewhere between the linear profile of the non-slip case and the constant deformation at all points given by the total-slip case. Once the pressure reaches the constant phase, the membrane in contact with the wall stretches further over time, hence generating significant displacements and relaxing the frictional forces.

5.3 Directional motion

To achieve directional motion we need the contact between wall and membrane to have anisotropic features. In other words the derived slip factor μ^* needs to be smaller in the forward, compared to the backward direction ($\mu^*_{forward} < \mu^*_{backward}$). This could be achieved if the droplet membrane had scales like the ones that fish or snakes have. That feature shall be represented in our model by different slip coefficients according to the direction of motion.

Figure 5.3: 3D graphical representation of the motion of a droplet undergoing 8 cycles of inflation-deflation with anisotropic slippage.

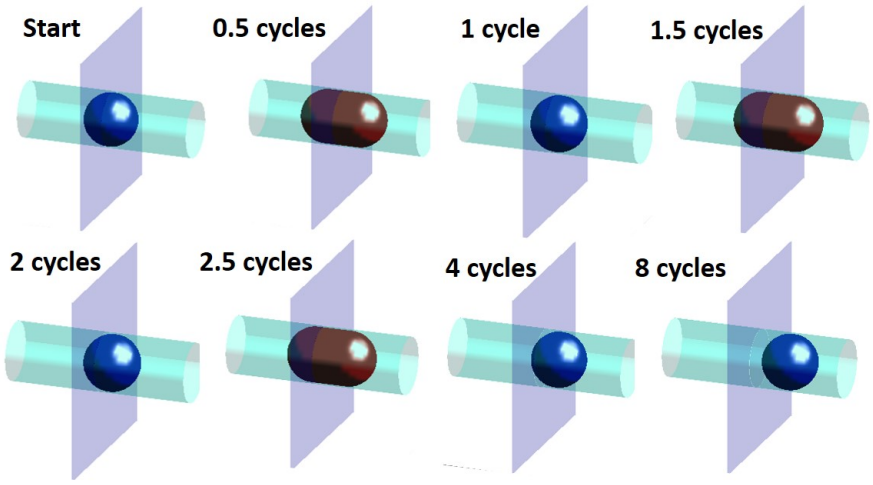

As a result, during the inflation phase the droplet grows because of: 1) the stretching of the membrane caps and 2) the slip of the portion of the membrane in contact with the wall. Hence the membrane will grow further in the direction in which the μ^* is smaller, leading to a shift in the center of mass. During the deflation phase, the droplet shrinks due to the relaxation of the caps. Simultaneously, the membrane wall will undergo further slip, resulting in the droplet shrinking faster in the direction in which μ^* is smaller, leading to further shift of the center of mass, as Figure 5.3 depicts.

Figure 5.4: Nondimensional pressure-time history (top) and evolution of the nondimensional center of mass (bottom) of a membrane with anysotropic friction

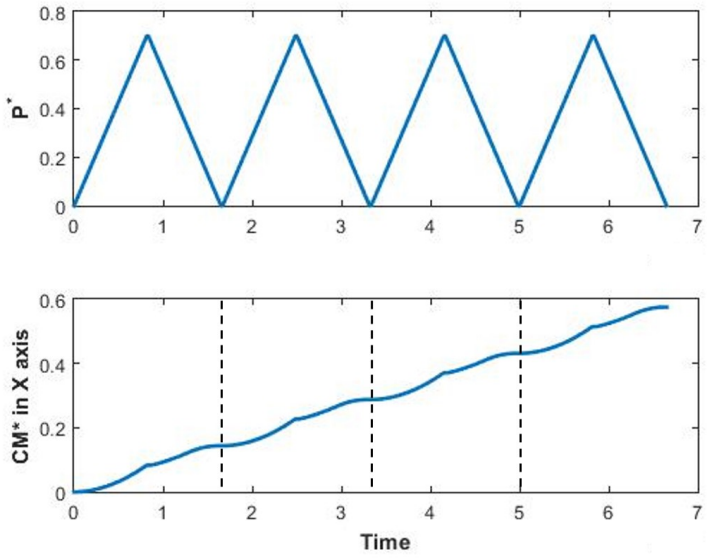

The capacity of the designed hydrogel to move in a straight channel depends mainly on two factors: 1) The amount of inflation and deflation and the duration of the cycles, 2) the anisotropy of the interaction between wall and body in both directions which is governed by the derived factor μ^*. Optimal gel design needs to yield a low μ^* in the forward direction and a high μ^* in the other, allowing it to crawl forward.

Other considerations that affect gel motion are the minimum and the maximum level of confinement of the gel. A confinement that is too high will not allow the gel to slip and one that is too low will leave the gel floating in an environment where viscous forces are dominant over inertial forces (low Reynolds), resulting in the maximum inflation of the gel to be inadequate for deposition with the wall.

Chapter 6

Formulation for a 3D Axisymmetric Domain and an Hyperelastic Membrane

6.1 Objectives

We wish to extend our problem to a 3D axisymmetric problem in which the material is described through the hyperelastic material model. The formulation we will develop is applicable to any channel shape in which the radius can be described as a function of the axial coordinate and for bodies in which the stress-free ends have a spherical or nearly-spherical shape. The problem is driven by the pressure difference between the inside and the outside of the droplet, and the channel shape is assumed to be known.

To simulate and study the behavior of this system, we will need to derive their governing equations, and these will depend on the deformation of the membrane. Hence the scheme to formulate the problem will be as follows:

(1) Establish the kinematics so that for any given reference and current shape we can compute the strain at each point of the membrane.

(2) Establish the relationship between strain and stress.

(3) Derive the governing equations.

The nature of the kinematics, relationship between strain and stress relationship and governing equations is significantly different whether we are looking at a point of the membrane that is in contact with the wall or at a point in the spherical caps that close the membrane at both ends. Consequently. we will derive both parts separately.

6.1.1 Kinematics

The goal of this section is to find the strain throughout the membrane as a function of the mapping between the reference and the current configuration. As we will show later, the strain and stresses are constant throughout the spherical caps; therefore, it will be useful to first find the mapping of the coordinates that separate the spherical caps from the membrane in contact with the wall.

In an axisymmetric domain, let us consider a closed membrane of initial shape Ω_0 which is defined according to a parametric curve $R = R(Z)$ and a current shape Ω whose geometry is described through $\mathfrak{z} = f(Z)$ and $r = f(Z)$. At any axial coordinate Z, we can define the tangent to the membrane surface by the angle α_0 in the initial configuration and α in the current. Both angles can be described as a function of the radius through $\tan(\alpha) = \frac{dR}{dZ}$. We will consider a non-wetting membrane, hence when it is in contact with the wall α matches the angle defined by the channel surface.

For convenience, we will work with the arc parameter S in the reference configuration and $\mathfrak{s}$ in the current configuration. We can exchange the axial and arc parameter through $Z(S)$ and $\mathfrak{z}(\mathfrak{s})$. Similarly, we will write the radius of the membrane and the angle between membrane and axial coordinate as a function of the arc parameter: $R(S)$, $r(\mathfrak{s})$, $\alpha_0(S)$ and $\alpha(\mathfrak{s})$.

Figure 6.1: Scheme of the membrane confined in a channel in initial and current configuration

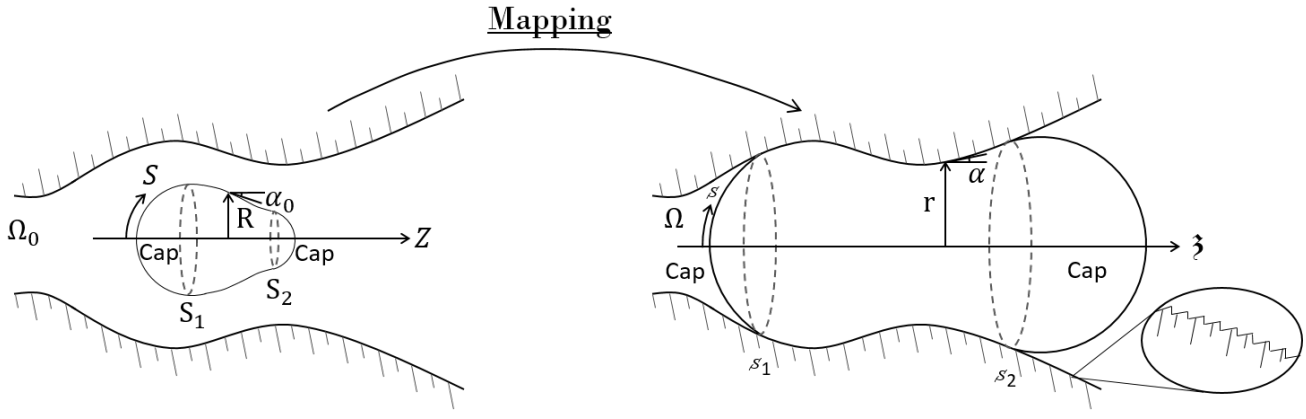

We are defining $\mathfrak{s}_1$ and $\mathfrak{s}_2$ as the coordinates of the membrane in the current configuration that separate the spherical caps from the channel. Both coordinates can be mapped back to the original configuration S_1 and S_2 respectively. While the membrane is not in contact at the deformed configuration, $\mathfrak{s}_1$ and $\mathfrak{s}_2$ match. As the membrane inflates on the channel walls, the reference coordinates S_1 and S_2 grow further away one from the other.

The geometry of the membrane in the initial shape is described by $R(S)$ while the geometry of the current shape is described by $\mathfrak{s}(S)$ and $r(S)$, which is prescribed by the channel shape in the contact area. The mapping between both states is fully described by the scalar-valued function $\mathfrak{s}(S)$ in $[S_1, S_2]$ and the coordinates S_1 and S_2, assuming that the channel shape, $r(S)$, is known as well as the $R(S)$.

$$S_1, S_2 \;\; and \;\; \mathfrak{s}(S) \quad in \quad [S_1, S_2] \tag{6.1}$$

6.1.1.1 Spherical caps mapping

This section will be devoted to writing the strain in the caps as a function of the mapping of the coordinates $\mathfrak{s}_1(S_1)$ and $\mathfrak{s}_2(S_2)$. A spherical cap in the reference configuration becomes a spherical cap in the current configuration, but the center of the cap's position changes; consequently, it is not a purely isotropic deformation. We will assume that the distortion will have a small impact on the stored elastic energy (derived further on) and so can be neglected. The coordinate system of a sphere is given by a radial coordinate perpendicular to the membrane and two angular in-plane coordinates (R, ϕ, θ). Enforcing incompressibility, we can express the deformation in the radial direction as a function of the in-plane directions; hence the deformation gradient:

$$\mathbf{F}(S_i) = \begin{pmatrix} 1/\lambda^2 & 0 & 0 \\ 0 & \lambda & 0 \\ 0 & 0 & \lambda \end{pmatrix} \tag{6.2}$$

Given that the membrane inflates isotropically, the deformation and stress in ϕ and θ are the same and equal at all points. To relate the mapping with the strain, we shall: 1) Compute the area of

the spherical caps in the reference and in the deformed configuration, and 2) Compare both areas to find the membrane strain in each spherical cap.

Figure 6.2: Scheme of spherical caps

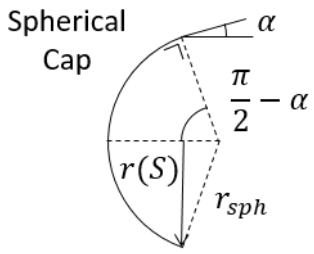

Given the coordinates $\mathfrak{s}_1$ and $\mathfrak{s}_2$, corresponding to the sections that separate caps from the wall, we can find, through the wall geometry, the radius of the caps $r(\mathfrak{z})$ as $r(\mathfrak{z}_1)$ and $r(\mathfrak{z}_2)$. Similarly, we can obtain the angle of the membrane at the given points. Then, the area of the spherical caps shall be computed as:

$$\mathcal{A}(r,\alpha) = \frac{2\pi r^2}{\sin\left(\frac{\pi}{2}-\alpha\right)}\left(\frac{1}{\sin\left(\frac{\pi}{2}-\alpha\right)} - \frac{1}{\tan\left(\frac{\pi}{2}-\alpha\right)}\right) \tag{6.3}$$

This formula is applicable for both the reference and the current configuration. Hence, $A_0 = \mathcal{A}(R,\alpha_0)$ and $A = \mathcal{A}(r,\alpha)$. With the strain, we can relate the spherical caps in the current state with the spherical caps at reference state. The Jacobian of the gradient of deformations of the in-plane coordinates yield the change in area, which in our case is equal to λ^2. Hence:

$$\lambda^2 = \frac{\mathcal{A}(r,\alpha)}{\mathcal{A}(R,\alpha_0)} \tag{6.4}$$

The situation of interest is when the membrane is partially in contact with the surrounding channel, which means that r and α are prescribed by the channel geometry, therefore a function of Z. As previously mentioned, we assume a non-wetting surface so that the membrane is tangent to the surface, hence $\tan(\alpha)$ is equal to $\frac{dR}{dZ}$. Resulting in $A = \mathcal{A}(r(S),\alpha(S)) = \mathcal{A}(Z)$. All in all, the area of the spherical caps in the current configuration, A, can be found as a function of S and along the strain state of the caps we can obtain A_0, the area of the caps in the reference configuration.

Therefore, we can write the strain at the caps as a function of Z, $\lambda_1(S_1)$ and $\lambda_2(S_2)$ through $\lambda_1(S_1) = \mathcal{A}(\mathfrak{s}_1)/\mathcal{A}(S_1)$ and $\lambda_2(S_1) = \mathcal{A}(\mathfrak{s}_2)/\mathcal{A}(S_2)$.

6.1.1.2 Membrane wall contact

Given the mapping of $\mathfrak{s}_1(S_1)$ and $\mathfrak{s}_2(S_2)$ and the strains at both caps, λ_1 and λ_2, we shall now tackle the derivation of the strains for $S_1 > S > S_2$ at the current configuration.

The nature of the problem is characterized by two strains: the strain that is tangential to the channel, λ_t, and the strain that is circular around the axis of symmetry, λ_θ. In the principal directions (t, θ, n), the gradient of deformation is a diagonal matrix. We assume that the membrane is incompressible, hence the Jacobian needs to be equal to one, and we can express the deformation in the normal direction as a function of the other deformations.

$$\mathbf{F}(S) = \begin{pmatrix} \lambda_t & 0 & 0 \\ 0 & \lambda_\theta & 0 \\ 0 & 0 & \frac{1}{\lambda_t \lambda_\theta} \end{pmatrix} \tag{6.5}$$

The circular strain is constrained by the channel shape, hence we can express it through the length of the circular perimeter in the current state and the related perimeter in the reference state.

$$\lambda_\theta(S) = \frac{L_\theta}{L_{\theta,0}} = \frac{2\pi r(\mathfrak{s}(S))}{2\pi R(S)} = \frac{r(\mathfrak{s}(S))}{R(S)} = g(S, \mathfrak{s}(S)) \quad in \quad [S_1, S_2] \tag{6.6}$$

Therefore, the circular strain λ_θ can be expressed as a function of the radius ratio mapping $g(S, \mathfrak{s}(S))$.

Let us now look at the tangential strain and mapping of the axial coordinate.

Figure 6.3: Scheme of the mapping of a section between reference and current state

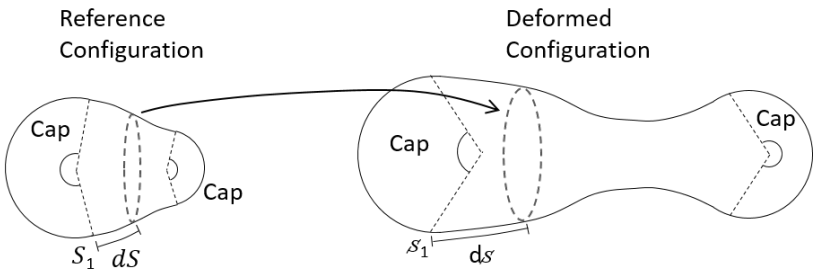

The mapping of the axial coordinate $\mathfrak{z}(Z)$ is given by the tangential stretching of the membrane $\lambda_t(S)$ through $ds = dS\lambda_t(S)$.

$$\frac{d\mathfrak{s}}{dS} = \lambda_t(S) \tag{6.7}$$

Additionally, given that $\mathfrak{s}_1(S_1)$ and $\mathfrak{s}_2(S_2)$ are known, if we knew λ_t we could map each point throughout the membrane-wall contact length as:

$$S = S_1 + \int_{S_1}^{S} d\mathfrak{s} = S_1 + \int_{S_1}^{S} \lambda_t dS \tag{6.8}$$

With that, we have derived a relationship between the mapping and the strain. Given a reference shape and a current shape, we can establish the relationship point to point through a strain function λ_t. In the following sections, we will elaborate upon the meaning of λ_t and how we can obtain it.

6.1.2 Coordinate system and principal directions

As the membrane inflates, it accommodates to the channel shape. Consequently, the principal directions are the tangential, the normal, and the circular. The forces acting on the membrane will be pressure normal to the channel, the surface tension and frictional forces parallel to it. Given that the membrane is very thin, there are no shear forces acting throughout its thickness, and if there were shear forces in the circular direction, the membrane would twist, breaking the axisymmetry.

Figure 6.4: Stress scheme in principal directions (left) and in axisymmetric coordinates (right)

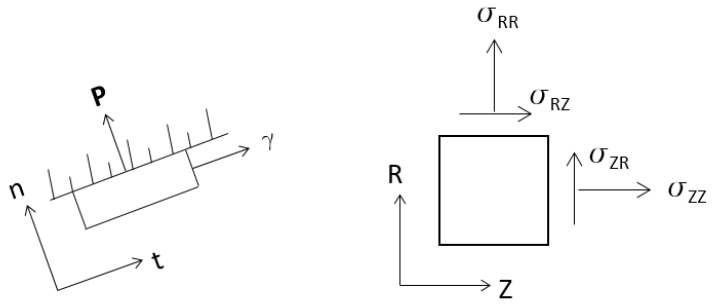

6.1.3 Strain and stress

In this section we will develop the relationship between strain and stress throughout the membrane. Note that the strain for the spherical caps and for the membrane in contact with the wall have been derived as a function of the mapping: $\lambda_1(S_1)$ and $\lambda_2(S_2)$ for the spherical caps, and $\lambda_\theta(g(S))$ and $\lambda_t(\mathfrak{s}(S))$ for the membrane wall.

6.1.3.1 At the membrane-wall contact

As previously stated, the gradient of deformation in the principal directions (t, θ, n) is given by:

$$\mathbf{F}(S) = \begin{pmatrix} \lambda_t & 0 & 0 \\ 0 & \lambda_\theta & 0 \\ 0 & 0 & \frac{1}{\lambda_t \lambda_\theta} \end{pmatrix} \tag{6.9}$$

As shown in the previous section, the circular deformation can be expressed as a function of the tangential deformation $\lambda_\theta(\lambda_t(S))$. Hence, the gradient of deformation throughout the membrane will be written as a function of the tangent deformation $\mathbf{F}(\lambda_t(S))$ and, ultimately, of the axial coordinate $\mathbf{F}(S)$.

The stored energy density function per unit of volume can then be computed:

$$\Psi = \frac{G_{sh}}{2}(tr(\mathbf{C}) - 3) = \frac{G_{sh}}{2}\left(\lambda_t^2 + \lambda_\theta^2 + \frac{1}{\lambda_t^2 \lambda_\theta^2} - 3\right) \tag{6.10}$$

Where $\mathbf{C}$ is the right Cauchy-Green deformation tensor, equal to $\mathbf{F}^T\mathbf{F}$. Now, we can compute the tangential stress:

$$P_{tt} = \frac{\partial \Psi}{\partial \lambda_t}\Big|_{\lambda_\theta = ct} = G_{sh}\left(\lambda_t - \frac{1}{\lambda_t^3 \lambda_\theta^2}\right) \tag{6.11}$$

The Cauchy in the tangential direction:

$$\sigma_{tt} = \frac{A_0}{A} P_{tt} = \frac{1}{\lambda_\theta \frac{1}{\lambda_t \lambda_\theta}} P_{tt} = G_{sh}\left(\lambda_t^2 - \frac{1}{\lambda_t^2 \lambda_\theta^2}\right) \tag{6.12}$$

The stress on the other directions are not of interest for the problem we are solving. Given σ_{tt}, we can compute the surface tension in the tangential direction as:

$$\gamma_t = \sigma_{tt} t = t G_{sh} \left(\lambda_t^2 - \frac{1}{\lambda_t^2 \lambda_\theta^2} \right) \tag{6.13}$$

Where t is the current thickness of the membrane, which we can write as:

$$t = t_0 \frac{1}{\lambda_t \lambda_\theta} \tag{6.14}$$

Hence, the tangential surface tension:

$$\gamma_t = t_0 G_{sh} \left(\frac{\lambda_t}{\lambda_\theta} - \frac{1}{\lambda_t^3 \lambda_\theta^3} \right) \tag{6.15}$$

6.1.3.2 At the spherical caps

Let us now formulate the strain-stress relationship in the spherical caps of the membrane, given the hyperelastic model. As previously stated, the strains are constant throughout the cap and the gradient of deformation in the (R, ϕ, θ) coordinate system can be written as:

$$\mathbf{F}(S_i) = \begin{pmatrix} 1/\lambda^2 & 0 & 0 \\ 0 & \lambda & 0 \\ 0 & 0 & \lambda \end{pmatrix} \tag{6.16}$$

Given that the membrane inflates isotropically, the deformation and stress in ϕ and θ are the same. For simplicity, we will call them $in-plane$ since they are tangent to the sphere surface. The elastic stored energy per unit of reference volume is then:

$$\Psi = \frac{G_{sh}}{2}(tr(\mathbf{C}) - 3) = \frac{G_{sh}}{2} \left(2\lambda^2 + \frac{1}{\lambda^4} - 3 \right) \tag{6.17}$$

The nominal stress in-plane is:

$$P_{in-plane} = \frac{\partial \Psi}{\partial \lambda} = 2 G_{sh} \left(\lambda - \frac{1}{\lambda^5} \right) \tag{6.18}$$

Then the Cauchy stress:

$$\sigma_{in-plane} = \frac{A_0}{A} P_{in-plane} = \frac{1}{\frac{1}{\lambda^2}\lambda} P_{in-plane} = 2 G_{sh} \left(\lambda^2 - \frac{1}{\lambda^4} \right) \tag{6.19}$$

Where A_0 is the reference area on which $\sigma_{in-plane}$ actuates and A the current deformed area. The current area is stretched in the radial direction by $\frac{1}{\lambda^2}$ and in the in-plane direction by λ.

Given $\sigma_{in-plane}$, we can compute the surface tension as we have previously done:

$$\gamma_{in-plane} = \sigma_{in-plane} t = 2tG_{sh}\left(\lambda^2 - \frac{1}{\lambda^4}\right) \tag{6.20}$$

Where t is the current membrane thickness, which we can write as a function of the reference membrane thickness:

$$t = t_0 \frac{1}{\lambda^2} \tag{6.21}$$

Hence:

$$\gamma_{in-plane} = 2G_{sh} t_0 \left(1 - \frac{1}{\lambda^6}\right) \tag{6.22}$$

6.2 Governing Equations

Now that we have written strain and stress in terms of the mapping unknowns S_1, S_2 and $\mathfrak{s}(S)$ in $[S_1, S_2]$, we shall derive the governing equations for both the spherical caps and the membrane-wall.

Figure 6.5: Stress scheme in principal directions (left) and in axisymmetric coordinates (right)

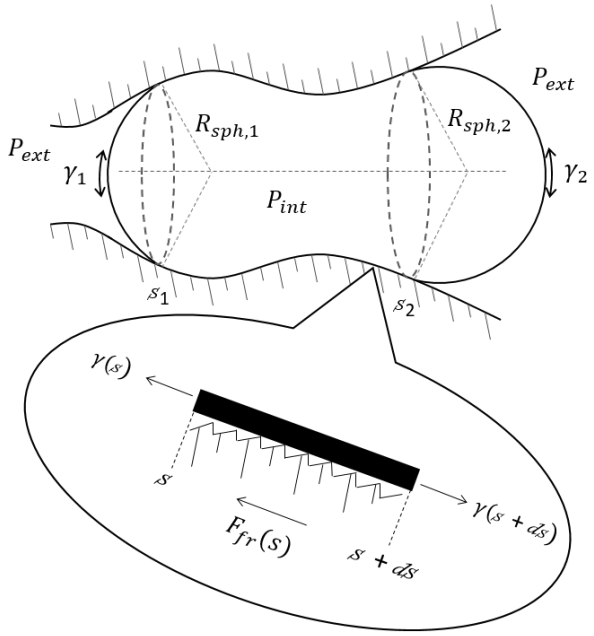

6.2.1 Spherical caps

Given that our problem is pressure driven, we shall apply Laplace's Law at each of the spherical caps:

$$\triangle P = \gamma_i \frac{2}{r_{sph,i}} \tag{6.23}$$

Where $\triangle P = P_{int} - P_{ext}$ and the spherical radius is given by $r_{sph,i} = \frac{r(\mathfrak{s}(S_i))}{\sin\left(\frac{\pi}{2} - \alpha_i\right)}$. Plugging in the derived expressions for the stress and the radius for the spherical caps S_1 and S_2:

$$\triangle P = \gamma(\mathfrak{s}(S_i)) \frac{2\sin\left(\frac{\pi}{2} - \alpha_i\right)}{r(\mathfrak{s}(S_i))} = 4Gt_0 \left(1 - \frac{1}{\lambda_i^6}\right) \frac{\sin\left(\frac{\pi}{2} - \alpha(\mathfrak{s}(S_i))\right)}{r(\mathfrak{s}(S_i))} \quad i = 1, 2 \tag{6.24}$$

Introducing in the derived equations of the strains at the caps: $\lambda_i^2(S_i) = \mathcal{A}(\mathfrak{s}(S_i))/\mathcal{A}(S_i)$:

$$\triangle P = 4G_{sh}t_0 \left(1 - \frac{1}{(\mathcal{A}(\mathfrak{s}(S_i)/\mathcal{A}(S_i))^3}\right) \frac{\sin\left(\frac{\pi}{2} - \alpha(\mathfrak{s}(S_i))\right)}{r(\mathfrak{s}(S_i))} \quad i = 1, 2 \tag{6.25}$$

Solving the equation and obtaining the coordinates S_1 and S_2 is very straight forward, and the application of a root finding algorithm suffices.

6.2.2 Membrane wall

Enforcing equilibrium of forces of a differential piece of membrane in contact with the wall as shown in figure XX yields:

$$\gamma(\mathfrak{s} + d\mathfrak{s}) - \gamma(\mathfrak{s}) - F_{fr}(\mathfrak{s})d\mathfrak{s} = 0 \tag{6.26}$$

Which we can rewrite as:

$$F_{fr}(\mathfrak{s}) = \frac{\gamma(\mathfrak{s} + d\mathfrak{s}) - \gamma(\mathfrak{s})}{d\mathfrak{s}} \tag{6.27}$$

When $d\mathfrak{s} \to 0$:

$$F_{fr} = \frac{\partial \gamma}{\partial \mathfrak{s}} \quad \text{in} \quad [\mathfrak{s}(S_1), \mathfrak{s}(S_2)] \tag{6.28}$$

$$F_{fr} = \frac{\partial \gamma}{\partial S}\frac{\partial S}{\partial \mathfrak{s}} = \frac{1}{\lambda_t}\frac{\partial \gamma}{\partial S} \quad \text{in} \quad [S_1, S_2] \tag{6.29}$$

Recall that we have previously derived the stress as $\gamma_t = \sigma_{tt} t_0$, and σ_{tt} has been derived in terms of the strains which in turn have been derived in terms of the mapping.

The interaction between wall and membrane is governed by the Maxwell model (a dashpot and a spring in series, connecting wall with membrane). Prior to writing the explicit equation for the interaction between wall and membrane, we shall remember that the difference between the current and the reference configuration is the displacement of the body.

$$u = \mathfrak{s} - S \tag{6.30}$$

Once the membrane gets into contact with the wall, it will start experiencing the interaction with the wall and, in turn, elastic and slip deformation. Hence, it is of our interest to separate the displacement previous and after the deposition of the membrane to the wall. We will write it as:

$$u(S,t) = u^D(S,t_d) + u^{MW}(S,t) \tag{6.31}$$

Where u^D is the displacement at time of deposition, equal to $\mathfrak{s}(S,t_d) - S$, and u^{MW} is the displacement due to the interaction between wall and membrane. We will prove that this definition

is consistent with the total displacement:

$$u^{MW}(S,t) = \mathfrak{s}(S,t) - \mathfrak{s}(S,t_d) = \mathfrak{s}(S,t) - S + S - \mathfrak{s}(S,t_d) = u(S,t) - u^D(S,t_d) \tag{6.32}$$

The interaction between wall and membrane is taken as a Maxwell model. Hence the frictional forces can be written as:

$$F_{fr} = \mu \dot{u}_s^{MW} \tag{6.33}$$

Assuming that the velocity of the elastic displacement, $\dot{u}_e^{MW}$ (due to the spring of the Maxwell model which is characterized by a very high coefficient), and the velocity of the displacement at contact, $\dot{u}^D$, are negligible in front of the slip velocity:

$$\dot{u} = \dot{u}_s^{MW} + \dot{u}_e^{MW} + \dot{u}^D \approx \dot{u}_s^{MW} \tag{6.34}$$

We can rewrite the previous equation as:

$$F_{fr} = \mu \dot{u} \tag{6.35}$$

And so the governing equation:

$$\mu \frac{\partial u}{\partial t} = \frac{1}{\lambda_t} \frac{\partial \gamma}{\partial S} \quad \text{in} \quad [S_1, S_2] \tag{6.36}$$

Where:

$$\mu(S) = \begin{cases} \mu^+, & \text{if } \dot{u}(S) > 0 \\ \mu^-, & \text{if } \dot{u}(S) < 0 \end{cases} \tag{6.37}$$

We can rewrite the governing equation as:

$$\mu \frac{\partial u}{\partial t} = \frac{t_0 G_{sh}}{\lambda_t} \frac{\partial}{\partial S} \left(\frac{\lambda_t}{\lambda_\theta} - \frac{1}{\lambda_t^3 \lambda_\theta^3} \right) \quad \text{in} \quad [S_1, S_2] \tag{6.38}$$

$$\frac{\mu}{t_0 G} \frac{\partial u}{\partial t} = \frac{1}{\lambda_t} \frac{\partial}{\partial S} \left(\frac{\lambda_t}{\lambda_\theta} - \frac{1}{\lambda_t^3 \lambda_\theta^3} \right) = \frac{1}{\lambda_t \lambda_\theta} \frac{\partial \lambda_t}{\partial S} - \frac{1}{\lambda_\theta^2} \frac{\partial \lambda_\theta}{\partial S} + 3 \left(\frac{1}{\lambda_t^5 \lambda_\theta^3} \frac{\partial \lambda_t}{\partial S} + \frac{1}{\lambda_t^4 \lambda_\theta^4} \frac{\partial \lambda_\theta}{\partial S} \right) \tag{6.39}$$

Rearranging the terms:

$$\frac{\mu}{t_0 G_{sh}} \frac{\partial u}{\partial t} = \left(\frac{1}{\lambda_t \lambda_\theta} + \frac{3}{\lambda_t^5 \lambda_\theta^3} \right) \frac{\partial \lambda_t}{\partial S} + \left(\frac{3}{\lambda_t^4 \lambda_\theta^4} - \frac{1}{\lambda_\theta^2} \right) \frac{\partial \lambda_\theta}{\partial S} \tag{6.40}$$

$$\frac{\mu}{t_0 G_{sh}}\frac{\partial u}{\partial t} = \left(\frac{\lambda_t^4\lambda_\theta^2 + 3}{\lambda_t^5\lambda_\theta^3}\right)\frac{\partial \lambda_t}{\partial S} + \left(\frac{3 - \lambda_t^4\lambda_\theta^2}{\lambda_t^4\lambda_\theta^4}\right)\frac{\partial \lambda_\theta}{\partial S} \tag{6.41}$$

Remember that the definition of the displacement is $u = \mathfrak{s} - S$. The initial configuration is independent of time, hence $\frac{\partial u}{\partial t}$ is equal to $\frac{\partial \mathfrak{s}}{\partial t}$. Recall also that:

$$\lambda_t = \frac{\partial \mathfrak{s}}{\partial S} \quad \text{in} \quad [S_1, S_2] \tag{6.42}$$

$$\lambda_\theta = \frac{r(\mathfrak{s})}{R(S)} \quad \text{in} \quad [S_1, S_2] \tag{6.43}$$

Hence:

$$\frac{\mu}{t_0 G_{sh}}\frac{\partial \mathfrak{s}}{\partial t} = \frac{R^3}{r^3}\left(\frac{\partial S}{\partial \mathfrak{s}}\right)^5\left(\left(\frac{\partial \mathfrak{s}}{\partial S}\right)^4\frac{r^2}{R^2} + 3\right)\frac{\partial^2 \mathfrak{s}}{\partial S^2} + \frac{R^4}{r^4}\left(\frac{\partial S}{\partial \mathfrak{s}}\right)^4\left(3 - \left(\frac{\partial \mathfrak{s}}{\partial S}\right)^4\frac{r^2}{R^2}\right)\frac{\partial \lambda_\theta}{\partial S} \tag{6.44}$$

With:

$$\frac{\partial \lambda_\theta}{\partial S} = \frac{1}{R(S)}\frac{\partial r}{\partial \mathfrak{s}}\frac{\partial \mathfrak{s}}{\partial S} - \frac{r(\mathfrak{s})}{R^2(S)}\frac{\partial R}{\partial S} \tag{6.45}$$

To prove the presented equation for the derivative of λ_θ through variations calculus:

$$R(S): \quad S + \delta S \to R(S) + \frac{\partial R}{\partial S}\delta S \tag{6.46}$$

$$\mathfrak{s}(S): \quad S + \delta S \to \mathfrak{s}(S) + \frac{\partial \mathfrak{s}}{\partial S}\delta S = \mathfrak{s}(S) + \lambda_t(S)\delta S \tag{6.47}$$

$$r(\mathfrak{s}(S)): \quad S + \delta S \to r(\mathfrak{s}(S)) + \frac{\partial r}{\partial S}\delta S = r(\mathfrak{s}(S)) + \frac{\partial r}{\partial \mathfrak{s}}\lambda_t \delta S \tag{6.48}$$

Hence:

$$\delta\lambda_\theta = \delta\left(\frac{r(\mathfrak{s})}{R(S)}\right) = \frac{\delta r(\mathfrak{s})R(S) - r(\mathfrak{s})\delta R(S)}{R^2(S)} = \frac{R(S)\frac{\partial r}{\partial \mathfrak{s}}\lambda_t - r(\mathfrak{s})\frac{\partial R}{\partial S}}{R^2(S)}\delta S \tag{6.49}$$

We can rewrite this as:

$$\frac{\delta\lambda_\theta}{\delta S} = \frac{1}{R(S)}\frac{\partial r}{\partial \mathfrak{s}}\lambda_t - r(\mathfrak{s})\frac{1}{R^2(S)}\frac{\partial R}{\partial S} \tag{6.50}$$

Returning to the governing equation; if we plug in the expression for $\frac{\delta\lambda_\theta}{\delta S}$ we obtain:

$$\frac{\mu}{t_0 G_{sh}}\frac{\partial \mathfrak{s}}{\partial t} = \frac{R^3}{r^3}\left(\frac{\partial S}{\partial \mathfrak{s}}\right)^5\left(\left(\frac{\partial \mathfrak{s}}{\partial S}\right)^4\frac{r^2}{R^2}+3\right)\frac{\partial^2 \mathfrak{s}}{\partial S^2} + \frac{R^4}{r^4}\left(\frac{\partial S}{\partial \mathfrak{s}}\right)^4\left(3-\left(\frac{\partial \mathfrak{s}}{\partial S}\right)^4\frac{r^2}{R^2}\right)\left(\frac{1}{R}\frac{\partial r}{\partial \mathfrak{s}}\frac{\partial \mathfrak{s}}{\partial S}-\frac{r}{R^2}\frac{\partial R}{\partial S}\right) \tag{6.51}$$

We can rearrange the equation and obtain:

$$\frac{\mu}{t_0 G_{sh}}\frac{\partial \mathfrak{s}}{\partial t} = \frac{R}{r}\frac{\partial S}{\partial \mathfrak{s}}\frac{\partial^2 \mathfrak{s}}{\partial S^2}+3\frac{R^3}{r^3}\left(\frac{\partial S}{\partial \mathfrak{s}}\right)^5\frac{\partial^2 \mathfrak{s}}{\partial S^2}+3\frac{R^3}{r^4}\left(\frac{\partial S}{\partial \mathfrak{s}}\right)^3\frac{\partial r}{\partial \mathfrak{s}} -3\frac{R^2}{r^3}\left(\frac{\partial S}{\partial \mathfrak{s}}\right)^4\frac{\partial R}{\partial S}-\frac{R}{r^2}\frac{\partial r}{\partial \mathfrak{s}}\frac{\partial \mathfrak{s}}{\partial S}+\frac{1}{r}\frac{\partial R}{\partial S} \tag{6.52}$$

Regarding the boundary conditions, they are given by the application of Laplace's law at both S_1 and S_2:

$$\frac{\partial \mathfrak{s}(S_i)}{\partial S} = \lambda_i \quad \text{for} \quad i = 1,2 \tag{6.53}$$

The initial value is set as the initial configuration plus the displacement in the previous time step and the displacement at time of deposition for the newly deposited material.

$$\mathfrak{s}(S,t_i) = S_i + u_{i-1} + u_i^D \tag{6.54}$$

We shall decompose the governing equation as:

$$\begin{cases} G(\lambda_t,\dot{\mathfrak{s}})\frac{\partial \mathfrak{s}}{\partial t} = H(\lambda_t)\frac{\partial \lambda_t}{\partial S} + I(\lambda_t) & \text{with } \lambda_t(S_i) = \lambda_{t,i} \text{ and} \\ \frac{\partial \mathfrak{s}}{\partial S} = \lambda_t, & \text{with } \mathfrak{s}(S_i) = u_i^D + S_i \text{ and } \mathfrak{s}(S,t_0) = S \end{cases} \quad \text{for } i = 1,2 \tag{6.55}$$

Where:

$$H(\lambda_t) = \frac{R}{r}\lambda_t^4 + 3\frac{R^3}{r^3} \quad I(\lambda_t) = 3\frac{R^3}{r^4}\frac{\partial r}{\partial \mathfrak{s}}\lambda_t^2 - 3\frac{R^2}{r^3}\frac{\partial R}{\partial S}\lambda_t - \frac{R}{r^2}\frac{\partial r}{\partial \mathfrak{s}}\lambda_t^6 + \frac{1}{r}\frac{\partial R}{\partial S}\lambda_t^5 \quad G(\dot{\mathfrak{s}},\lambda_t) = \frac{\mu\lambda_t^5}{t_0 G_{sh}} \tag{6.56}$$

6.2.3 Initial value: displacement at time of deposition "u^D"

As mentioned in the previous section, the initial displacement for the newly deposited material is the displacement at time of deposition $u^D(S, t_d)$. In this section, we will derive it. We will assume that in a given step, $\triangle S$ is the newly-deposited membrane material. From the previous step, we know the displacement at contact throughout the material that has already been deposited. Hence we only need to derive u^D for the newly deposited material. Consider this to be $[S_a, S_b]$. We will utilize the Taylor's expansion.

$$u^D(S_b, t_d) = u^D(S_a, t_d) + \left[\frac{\partial \mathfrak{s}}{\partial S}\right] dS + \frac{1}{2}\left[\frac{\partial^2 \mathfrak{s}}{\partial S^2}\right] dS^2 + H.O.T. \tag{6.57}$$

The strain at S_b is known from application of Laplace's Law. We will ignore high order terms and approximate the derivatives of the current configuration through the strain:

$$u^D(S_b, t_d) = u^D(S_a, t_d) + \lambda_{t,S_b} dS + \frac{1}{2}\frac{\lambda_{t,S_b} - \lambda_{t,S_a}}{\triangle S} dS^2 \tag{6.58}$$

6.3 Numerical solution to the governing equation

We will solve the derived governing equation through the application of finite differences method, more specifically the backward Euler method. Both time and space variables shall be discretized and each derivative in the PDE approximated through finite difference.

Let u_j^k denote the approximate solution at $S_j = j \triangle S$ and $t_k = k \triangle t$. We will replace the time derivative by a forward difference and the space derivatives by a centered difference. Note that given that the domain in which we solve the PDE is $[S_1, S_2]$ $\triangle S = (S_2 - S_1)/(n+1)$.

$$\begin{cases} G\left(\lambda_{t,i}^{k+1}, \mathfrak{s}_j^{k+1}, \mathfrak{s}_j^k\right) \frac{\mathfrak{s}_j^{k+1} - \mathfrak{s}_j^k}{\triangle t} = H(\lambda_{t,i}^{k+1}) \frac{\lambda_{t,i+1}^{k+1} - \lambda_{t,i-1}^{k+1}}{2\triangle S} + I(\lambda_{t,i}^{k+1}) \\ \frac{\mathfrak{s}_{j+1}^{k+1} - \mathfrak{s}_{j-1}^{k+1}}{2\triangle S} = \lambda_{t,i}^{k+1} \end{cases} \tag{6.59}$$

The boundary conditions:

$$\frac{\mathfrak{s}_2^{k+1} - \mathfrak{s}_1^{k+1}}{\triangle S} = \lambda_1^{k+1} \tag{6.60}$$

$$\frac{\mathfrak{s}_n^{k+1} - \mathfrak{s}_{n-1}^{k+1}}{\triangle S} = \lambda_2^{k+1} \tag{6.61}$$

Regarding the initial value:

$$\mathfrak{s}(S_j, t_1) = S_j \qquad j = 1, ..., n \tag{6.62}$$

The proposed backward Euler scheme is set up so that the configuration at time instant t_{k+1} can be obtained implicitly: $\mathfrak{s}_j^{k+1}$ for $j = 1, ..., n$. Given that our backward Euler formulation yields an implicit set of equations, we applied a root-finding algorithm to solve it–specifically, the "fsolve" algorithm of MATLAB.

Chapter 7

Membrane Motion Model: Analysis and Discussion

In this chapter we will analyze and discuss the results of the model defined in the previous chapter.

7.1 Convergence

To validate the precision of our simulations we will study how the time steps and element size converge to a solution. The key output parameter whose convergence we will analyze is the shift of the center of mass over an inflation-deflation cycle for a swelling ratio of about 2. Given that we do not have an analytic solution for that problem, our approach will consist on looking at ratios of differences between $\hat{u}_h$ (numerical solution for a small parameter h) computed for different h. We will compare solutions where h is halved successively from which we will be able to derive the order of convergence p. Schematically this can be represented as:

$$\frac{\hat{u}_h - \hat{u}_{h/2}}{\hat{u}_{h/2} - \hat{u}_{h/4}} = 2^p + O(h) \tag{7.1}$$

7.1.1 Time step convergence

Our governing equation is a partial differential equation in time and space, hence we will look at the convergence of both fields. We shall start by looking at how changing the number of time steps affects the precision of the solution.

Figure 7.1: Error in the shift of the center of mass over an inflation-deflation cycle against number of time steps for the full cycle in logarithmic scale

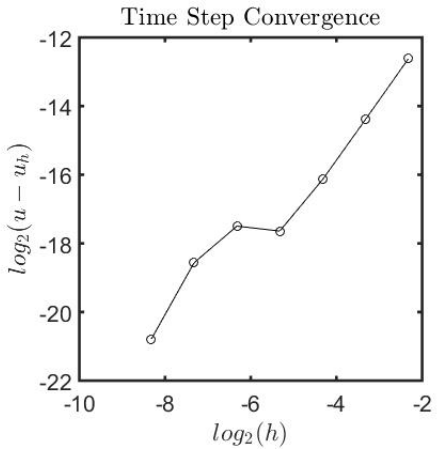

The order of convergence for the time steps has been calculated as 1.8. Beyond a step size of 1/200 the solution barely changes; hence, we will consider that this number of steps provide sufficient precision.

7.1.2 Element size convergence

We shall study how the number of elements (in which we divide the contact length between wall and membrane) affects the precision of the solution.

Figure 7.2: Error in the shift of center of mass over an inflation-deflation cycle against number of elements in contact between wall and membrane in logarithmic scale

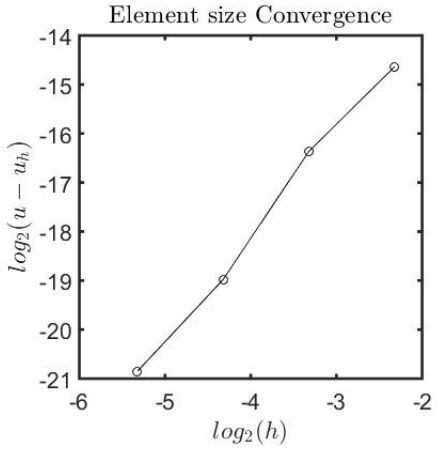

In this case the solution order of convergence with element size is of about 1.5. Note that if we keep halving our solution the computational cost increases very rapidly. We will consider that for an element size of 1/50 the solution precision is satisfactory.

7.2 Nondimensionalization

As we previously did for the linear elasticity membrane confined in a straight channel, we shall transform our variables so that we can work with dimensionless parameters. This will help us assess the relative importance of the terms in the model equations and facilitate the scale-up of the obtained results. Given that the governing equations for our current case are significantly complex, the derived non-dimensional number would fail to allow us to understand the importance of terms in a straight-forward and easily understandable way. Hence, instead of nondimensionalizing the governing equations we shall adapt the previously derived slip factor "μ^*" to our model.

For a membrane with a hyperelastic strain-stress constitutive equation with a channel whose geometry is described through $R(\mathfrak{s})$, the nondimensionalized variables we shall be written as:

$$t^* = \frac{\dot{P}R_0}{G_{sh}h_0}t \quad u^* = \frac{u}{R_0} \quad S^* = \frac{S}{R_0} \quad P^* = \frac{R_0}{G_{sh}h_0}P \tag{7.2}$$

Where R_0 is the membrane radius at the reference configuration. Adapting the slip factor "μ^*" from the previous simple model to our case yields:

$$\mu^* = \frac{\dot{P}\mu R_0^3}{(G_{sh}h_0)^2} \tag{7.3}$$

We expect that if μ^* increases, the system will undergo less slip, and if it decreases, more slip as is shown in the elastic straight channel case.

7.3 μ^*_{mean} and μ^*_{ratio}

For the membrane to move, the contact needs to be characterized by a low μ^* in the direction we want the body to move and a high μ^* in the opposite. Doing so will allow the gel to slip against the wall in the forward direction and stick in the opposite.

The interaction between wall and membrane can be summarized through two parameters: μ^*_{mean} and μ^*_{ratio}.

$$\mu^*_{mean} = \frac{\mu^*_{forward} + \mu^*_{backward}}{2} \tag{7.4}$$

$$\mu^*_{ratio} = \frac{\mu^*_{forward}}{\mu^*_{backward}} \tag{7.5}$$

μ^*_{ratio} accounts for the anisotropy so that if $\mu^*_{ratio} = 1$ the contact is isotropic and there is no directional motion. μ^*_{mean} tells us about the slippage the system undergoes. These ideas will be developed later in this chapter.

7.4 Benchmark problems

To verify that the obtained solutions are correct we will look at a few benchmark problems for which the solution is known. We will verify that the displacement and strain fields are correct by comparing the numerical solution to the analytic.

7.4.0.1 High μ^*

In a case where there is no slip, as the membrane inflates a larger portion of the membrane comes into contact with the wall, and each point that comes into contact with the wall is characterized by a known deformation (thanks to Laplace's law). Given that we are considering a stick case, the membrane is not allowed to slip further once it comes into contact with the wall. All together, the obtained displacement field is given by the derived displacement at time of deposition "u^D".

For the case of a straight channel, the analytic solution for the displacement can be derived as:

$$u(S) = aS + bS^2 \tag{7.6}$$

$$\lambda = \frac{du}{dS} + 1 = a + 2bS + 1 \tag{7.7}$$

With boundary conditions:

$$\lambda(S = 0) = \lambda_{contact} \tag{7.8}$$

$$\lambda(S = S_{end,-}, S_{end,+}) = \lambda_{cap} \tag{7.9}$$

Which yields:

$$\lambda(S) = \lambda_{contact} + S\frac{\lambda_{cap} - \lambda_{contact}}{S_{end}} sign(S) \tag{7.10}$$

And:

$$u(S) = (\lambda_{contact} - 1)S + \frac{\lambda_{cap} - \lambda_{contact}}{2S_{end}} S^2 sign(S) \tag{7.11}$$

For the case of an inclined channel, the analytic solution for the displacement can be derived as:

$$u(S) = \begin{cases} a(S - S_{int}) + b_1(S - S_{int})^2, & \text{if } S_1 > S > S_{int} \\ a(S - S_{int}) + b_2(S - S_{int})^2, & \text{if } S_{int} < S < S_2 \end{cases} \tag{7.12}$$

Solving for a, b_1, b_2 using the known strain at the caps and at time of first contact with the wall:

$$u(S) = \begin{cases} (\lambda_{contact} - 1)(S - S_{int}) - \frac{\lambda_{cap,1} - \lambda_{contact}}{2(S_1 - S_{int})}(S - S_{int})^2, & \text{if } S_1 > S > S_{int} \\ (\lambda_{contact} - 1)(S - S_{int}) - \frac{\lambda_{cap,2} - \lambda_{contact}}{2(S_2 - S_{int})}(S - S_{int})^2, & \text{if } S_{int} < S < S_2 \end{cases} \tag{7.13}$$

Figure 7.3: Set of benchmark tests for a high μ^*. Pressure-time history (top left), scheme of the membrane arc parameter S along the strains (top right), numerical and analytical strains and displacements for a membrane inflating in a conical channel (A,B,C)

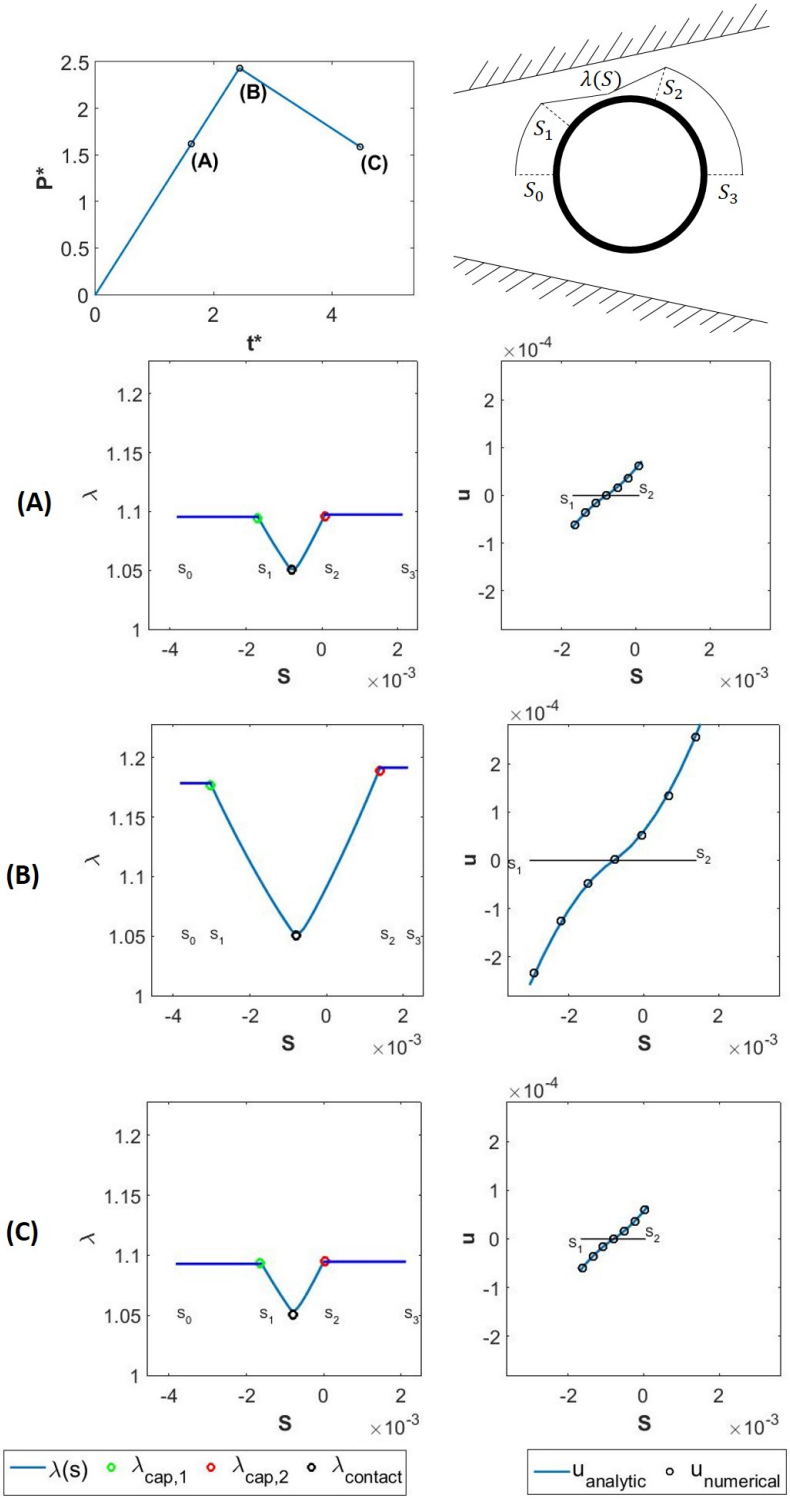

7.4.1 Low μ^* with straight walls

In the case where the membrane deforms freely when in contact with the wall, the strain all through it will be the same given by Laplace's law at the cap. Hence for the case of straight walls:

$$u(S) = (\lambda_{cap} - 1)S \tag{7.14}$$

Figure 7.4: Set of benchmark tests for a low μ^*. Pressure time history (top left), scheme of the membrane arc parameter S along the strains (top right), numerical and analytical strains and displacements for a membrane inflating in a straight channel (A,B,C)

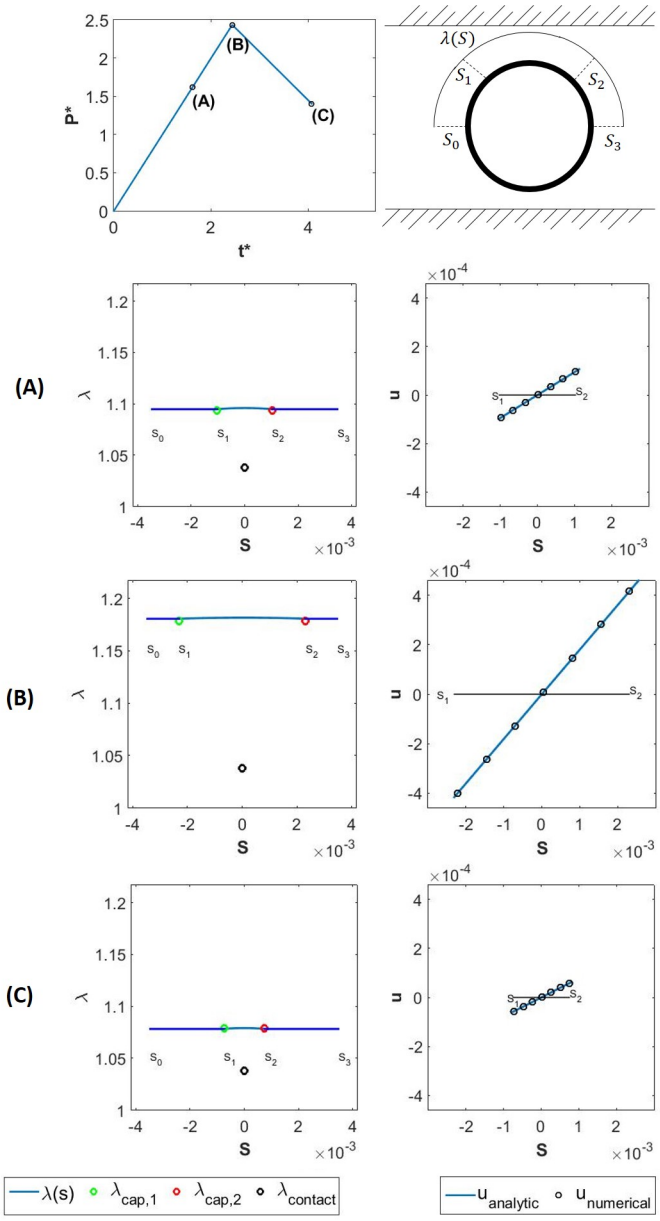

7.4.2 Slip case inclined walls

In the case of inclined walls, when the membrane comes into contact with the wall it simply slips so that it remains a sphere tangent to the wall. To confirm that the results are correct, we will perform a set of tests with different wall inclination and maximum achieved pressure for which we

can analytically find which is the position of the center of mass and compare to see if the results match.

The analytic solution will be given by the equation governing the free inflation of an sphere with a hyperelastic constitutive equation and the inclination of the wall. The free inflation equation is given by:

$$\frac{PR_0}{4h_0G_{sh}} = \frac{1}{\lambda} - \frac{1}{\lambda^7} \tag{7.15}$$

From this equation we obtain the strain λ and the radius is given by $R = \lambda R_0$. Given that this benchmark test is performed on straight inclined walls, we can easily compute the position of the center of mass:

$$X_{cm} = \frac{R}{\sin(\alpha)} - \frac{y_0}{\tan(\alpha)} \tag{7.16}$$

Figure 7.5: Scheme of the shift of center of mass for a low μ^* case

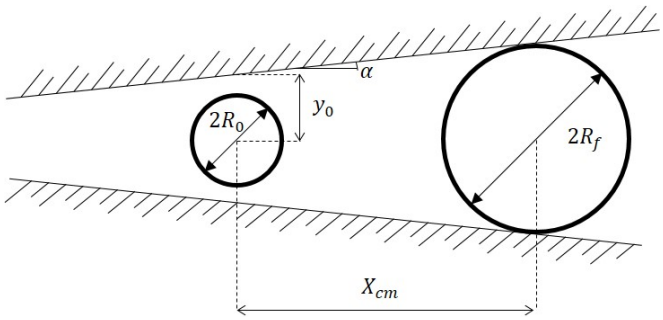

Figure 7.6: Numerical and analytic position of the center of mass for a membrane inflating in an inclined wall with slip conditions

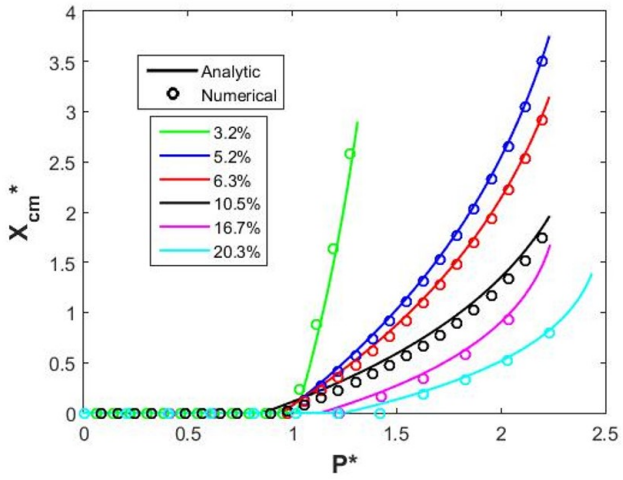

7.5 Mid μ^*: Membrane relaxation

A relevant feature we shall investigate to further validate the model is the relaxation of the membrane in contact with the wall over time. Figure 6.4 shows how the displacements behave according to different μ^* in a straight channel. For the case of a large μ^* the displacements are limited to the deformation of the caps, while in the case of a small μ^*, the membrane in contact with the wall completely slips so that the deformation at the wall matches the one at the caps, allowing for the largest possible displacements. In the case of a mid μ^* the membrane will experience further displacements during the constant pressure phase and the deformation field on the membrane-wall contact will slowly evolve towards the cap deformation.

Figure 7.7: Maximum displacement of a membrane (top) inflated in a straight channel through a ramp pressure loading followed by a constant pressure phase in a straight channel. Strains at the wall-membrane contact at different times for the mid μ^* case (bottom).

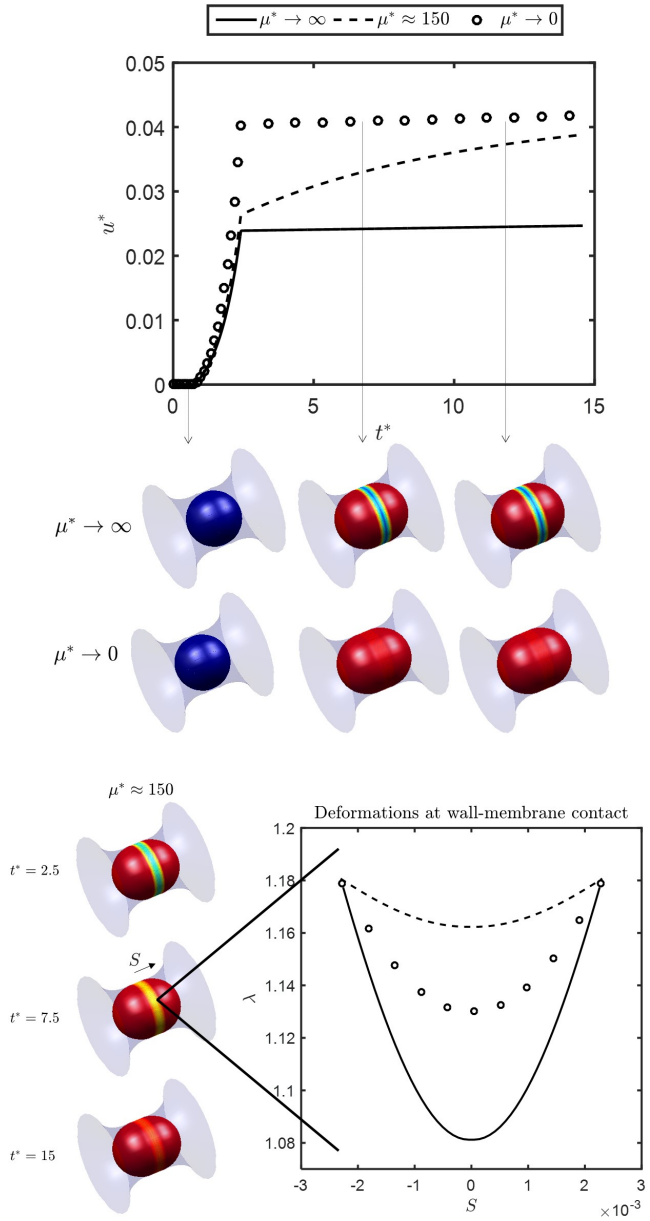

7.6 Directional motion

The factors that drive gel motion shall be summarized as: 1) the anisotropy of the interaction between wall and body in both directions which can be described through μ^*_{ratio} 2) the amount of

slip the body undergoes which is characterized through μ^*_{mean} 3) The confinement of the body . We shall write that the nondimensionalized velocity (displacement per cycle) is a function of:

$$v^* = f(c, \mu^*_{mean}, \mu^*_{ratio}) \tag{7.17}$$

7.6.1 μ^*_{ratio} effect on directional motion

μ^*_{ratio} governs the anisotropy of the system. The following picture depicts three cases of a spherical body undergoing periodical inflation deflation. Note that the center of mass of the body with $\mu^*_{ratio} = 1$ remains static while for the other cases it does not.

Figure 7.8: Effect of μ^*_{ratio} on directional motion

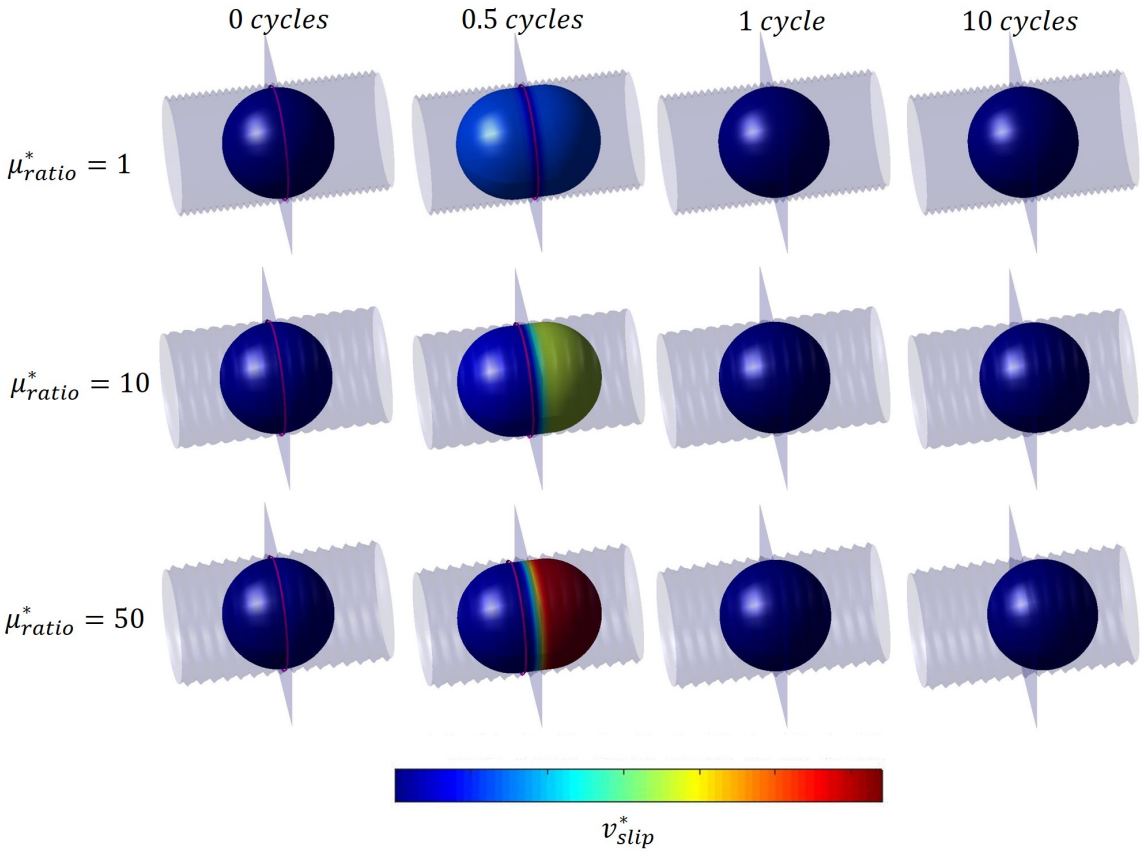

Note that our numerical experiments are pressure driven, this limits our capacity of swelling since

we cannot undergo softening. As a result the total motion per inflation-deflation cycle is small, however we can clearly see the displacement of the body over a larger number of cycles.
The purple ring represents the location of zero slip velocities, we shall call this point "anchor circle", we will develop this idea later in this chapter.

7.6.2 μ^*_{mean}: rolling versus slippage

As the membrane inflates new material deposits into the wall. Each piece of the membrane is stretched and then deposited. This rolling effect significantly decreases the amount of motion the sphere can achieve compared to a system that does not experience rolling such as a cylindrical body with axial inflation. The sphere spends a significant amount of energy in inflating and depositing already stretched material, this material will not be able to undergo large slippage since it is already stretched. Given that the rolling effect is symmetric it does not provide directional motion hence diminishing the efficiency of the spherical geometry compared to the cylindrical.
μ^*_{mean} shows the speed the membrane undergoes slip. For a low μ^*_{mean} the membrane starts slipping right after being deposited while for a high μ^*_{mean} the membrane slips very slowly.

Figure 7.9: Effect of μ^*_{ratio} on rolling and slippage, in color code the slip velocity

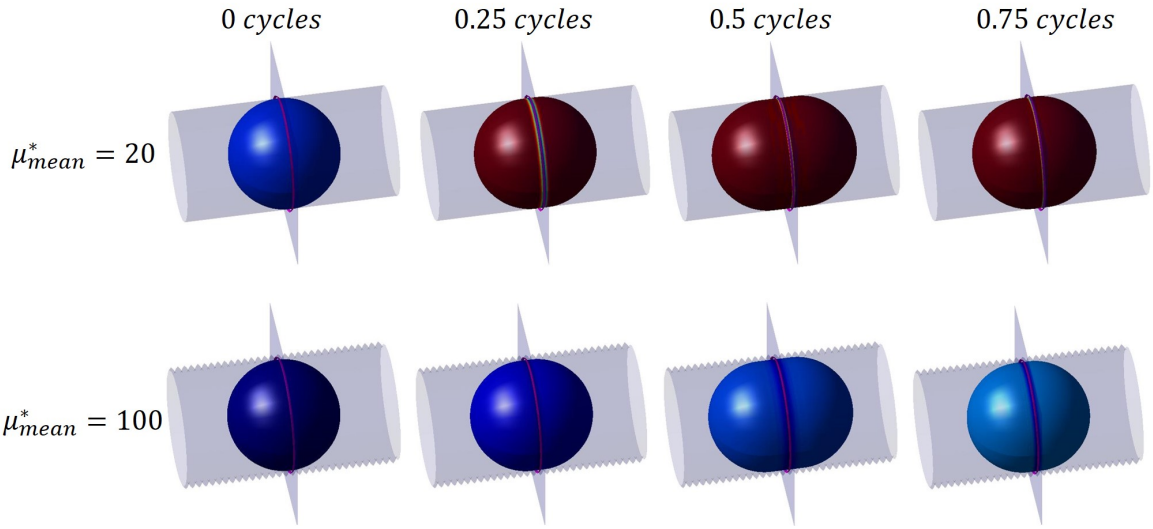

7.6.3 Confinement effect on directional motion

The amount of inflation and deflation while the body is confined is represented by the parameter c, already defined as $c = R^s/R_{ch} - 1$ (where R^s is the radius of the stress-free membrane with the same volume as the confined membrane). The body can move because the interaction forces between the channel and the body are not symmetric. Hence, maximizing the area of contact between channel and body will allow for a greater motion.

7.6.4 Anchor circle

A key element in directional motion is the point of zero slip velocities. We shall call this point (or circle in axisymmetric coordinates) the anchor. When the anchor circle is at the center of the body the system slips symmetrically leading to no directional motion (see figure 7.9). Directional motion is maximized when the circle of zero slip velocity is at the end of the contact between wall and membrane during the inflation and at the opposite end during the deflation.

Figure 7.10: Anchor circle (purple) on an anisotropic system at different times of the inflation-deflation cycle

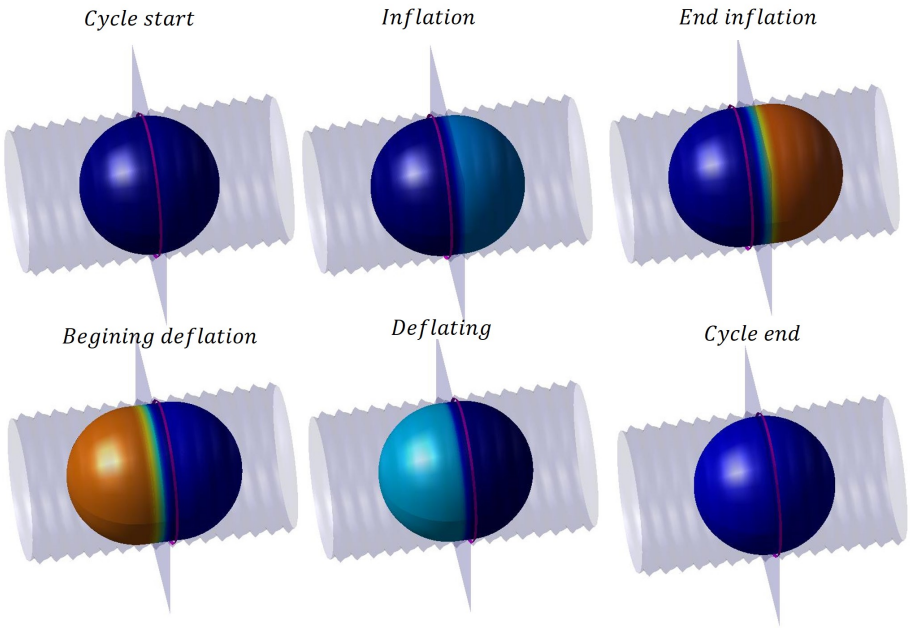

Chapter 8

Empirical Testing: PNIPAm Gel Motion in Porous Media

8.1 Introduction

To study the feasibility of PNIPAm gel motion in porous media, we have performed a set of empirical tests. These experiments were conceived as part of a high school science project. We collaborated with a student, Anurag Golla, to help him produce a science project about gel motion for targeted drug delivery which allowed us to outreach to the community.

Anurag presented the project in the INTEL ISEF (International Science and Engineeering Fair), and ranked first in the Boulder regional competition, the Corden Pharma Boulder Valley Regional Science Fair.

8.2 Experiment description

To study the feasibility of gel motion in porous media, we placed gels whose volume we could control remotely inside channels with different geometries (straight and tortuous with different wave length and amplitude) which had a ratchet on their surface providing anisotropic friction. The ratchet would account for the coating the gel would have so that it could move; given that the gel coating process is very challenging, we simply designed the channels with ratchets. The channel's tortuousness aims to represent the shape of a porous channel. These set of experiments allowed us to study the effect of confinement, ratchet geometry and porous media geometry on the speed of periodically inflating-deflating gels. Two types of tests were performed: passive (pressure driven) and active (volume driven).

8.3 Methodology

We synthesized PNIPAm monomer based gels of a cylindrical shape of about 1 cm length and 1 cm radius. The channels were designed and printed with 3D Lulzbot printers using t-glase filament. T-glase filament is a stiff material partially transparent which allowed us to see through and study the motion mechanics of the gel.

Figure 8.1: Channel models schematics for 3D printing, straight with ratchet (top), undulating (bottom)

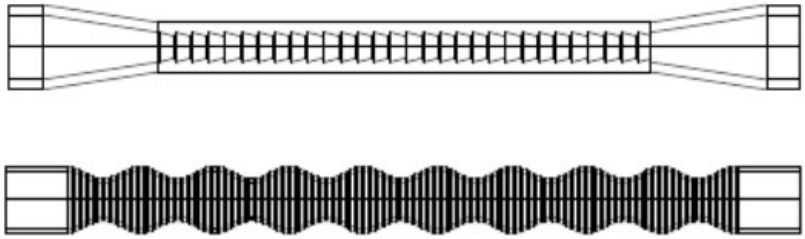

Figure 8.2: Printing of a tortuous channel with t-glase filament in a Lulzbot printer

Volume of PNIPAm gels are controlled through their temperature. They are characterized by a LCST (lower critcal solution temperature) near 32 celsius degrees around which their volume changes drastically. Hence, we submerged the gel in water and used tea heaters (metallic rod resistors) to control the temperature.

We performed two types of tests: passive in which the motion of the gel was obtained through a difference in pressure throughout the channel, and active in which the temperature was controlled.

8.3.1 Passive test

We set up a circuit to test the passive motion of gels (see figure below). Pressure was controlled by adding a known amount of water to one of the deposits. As a result, gels in the channel would experience a directional pressure that would move them and we could quantify the time it takes for them to go from one end of the channel to the other.

Figure 8.3: Passive test setup

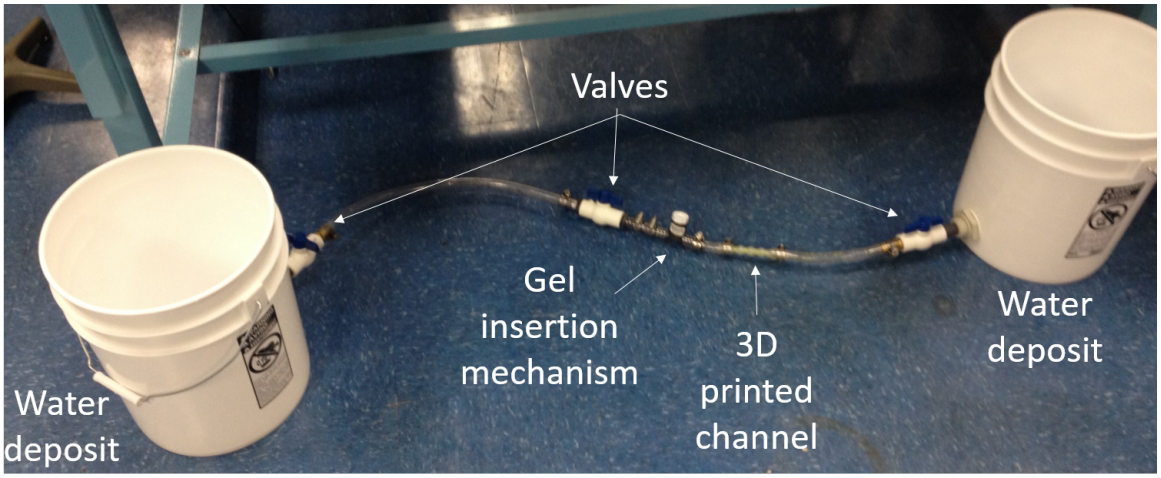

This type of experiment is particularly useful to study the effect of confinement on gels. As the gel is subjected to a larger confinement, the frictional forces increase and the speed the gel travels through the channel decreases. Passive tests are also very useful in studying the anisotropy of the ratchet. By measuring the velocity of the gel in both directions, we can compute the difference of velocities and determine an optimal ratchet geometry.

One key advantage of the passive test over active is that the former is much faster and facilitates easier data collection.

8.3.2 Active test

The active tests were performed by submerging a channel inside a water deposit like the ones in the previous figure. The water was heated up with a resistor and we let it cool down to room temperature to achieve the volume oscillation. If we were to do this in the passive test setup, we could potentially generate a gradient of temperatures through the channel, consequently distorting the motion mechanism and the subsequent results.

Figure 8.4: Schematics of the active test setup

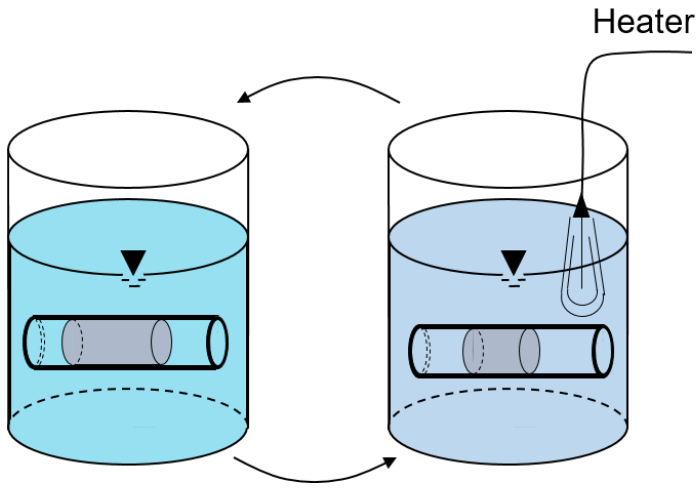

8.4 Active PNIPAm gel motion

To further illustrate the experiments we performed we shall include photographic documentation. Figure 8.5 shows the gel inside the channel in different inflation states. Figure 8.6 shows the position of the gel inside the channel after a number of inflation-deflation cycles. As we can observe for the case of a isotropic surface the gel does not move while in the case of an anisotropic surface we can clearly see a trend.

Figure 8.5: Confined PNIPAm gel inflation-deflation. Contour lines of the gel in white. Photographs and graphic production by Anurag Golla.

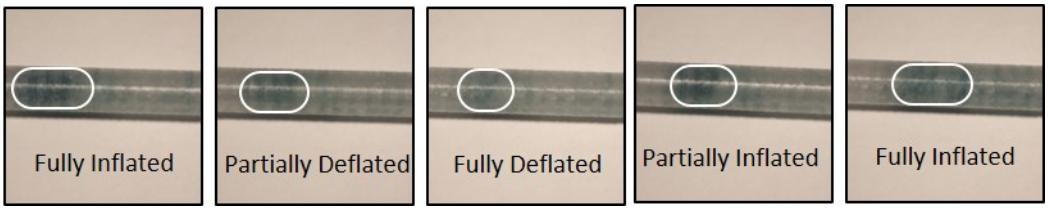

Figure 8.6: PNIPAm gel photographs showing motion in isotropic an anisotropic conditions. Photographs and graphic production by Anurag Golla.

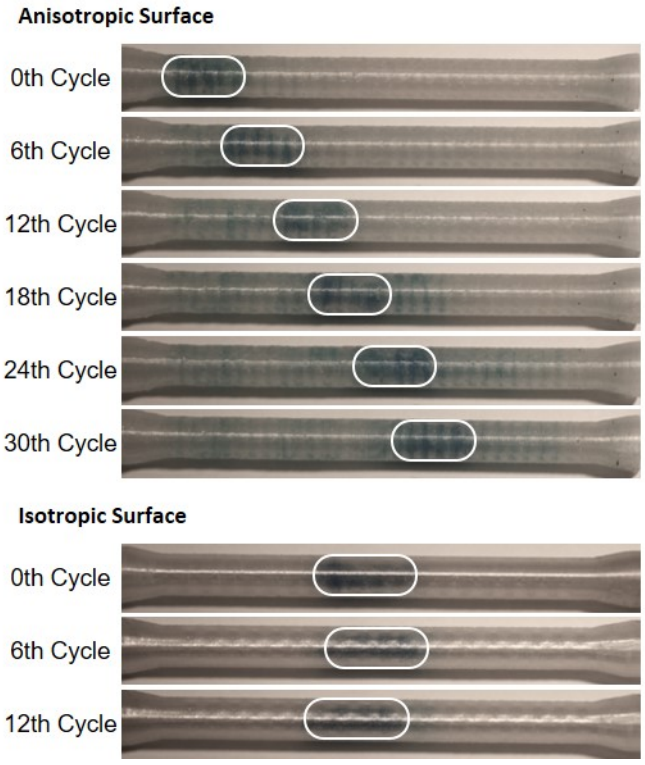

8.5 Results

8.5.1 Confinement

The first feature we studied was the gel deformability through confinement tests. We placed gels in straight channels of different diameters, because of the ability of PNIPAm gels to change their volume, we were able to generate very confined conditions. The results show that as the

confinement increases (gel diameter over channel diameter) the pressure necessary to move the gel increases exponentially. The gel did exhibit a significant deformability while maintaining its structural integrity; the added pressure necessary to move the gel when it was confined at 1,10 was about twice of the necessary pressure to move it when gel and channel diameters match.

Note that gel deformability can be tuned through different cross-link density formulations. However, a cross-link density that is too low would allow for greater deformability and would also decrease the gel strength, and so its integrity. It is a trade-off case of deformability versus strength.

Figure 8.7: Confinement test: critical pressure necessary to move the gel in passive test. Points are the empirical results and the line the exponential fit. Empirical results collection and graphic production by Anurag Golla.

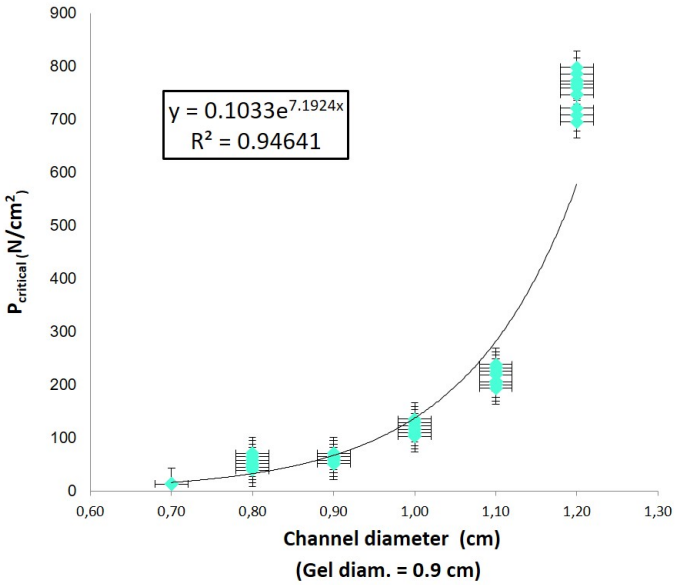

8.6 Ratchet design

A key aspect for gel motion is the capacity of the gel coating to generate anisotropic contact interaction with the wall. To study this phenomena, we designed channels with a ratchet on its inside surface.

Figure 8.8: Gel speed in straight channels in both directions when subject to a difference in pressure. D1 and D2 stand for both (and opposite) directions the gel can travel. Empirical results collection and graphic production by Anurag Golla.

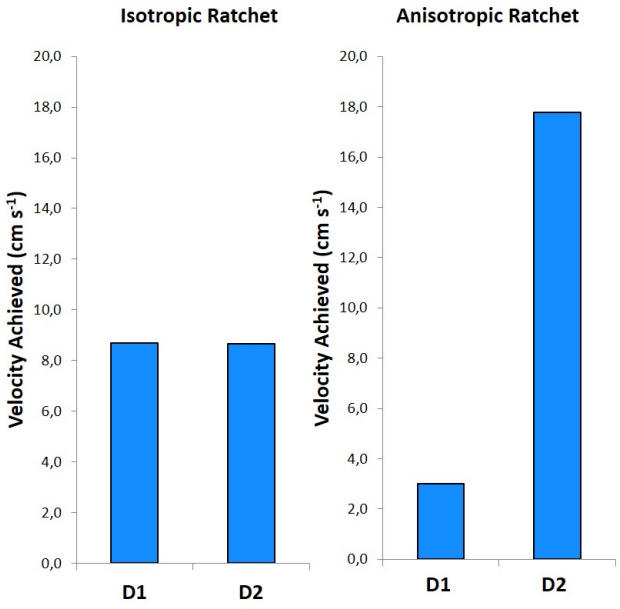

We also performed active tests to validate that the gels are able to move on their own. We placed the gel in straight channels with different ratchet geometries and performed active tests. Through increment and decrement of temperature, the gel volume oscillates, coupled with anisotropic friction forces provided by the ratchets, the gel moves. We measured the velocity of the gel on different ratchet geometry. The legend on the following figure (C1, C2, C3, C4) refers to the channel ratchet geometry. The ratchet width is 0.4 cm for C1, 0.8 for C2 and 1.0 for C3 and C4. The ratchet height is 0.08 cm for C1, C2 and C3 and 0.10 cm for C4. The control channel has no ratchet.

Figure 8.9: Gel speed in straight channels in both directions when subject to a difference in pressure. D1 and D2 stand for both (and opposite) directions the gel can travel. Empirical results collection and graphic production by Anurag Golla.

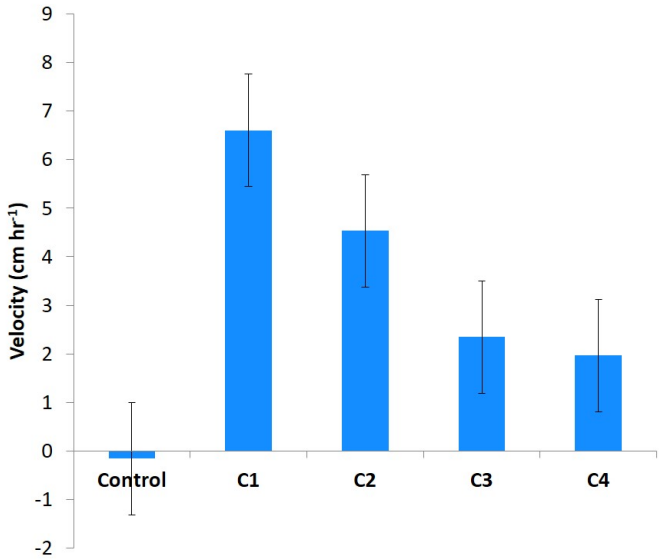

Note that the error bar for C3 and C4 overlap significantly; hence, comparison between both is not applicable. From this test, we can conclude that as the ratchet width decreases, the gel moves faster.

8.7 Conclusions

The main goal of this side project was to outreach to the community some of the challenges targeted drug delivery is facing. We were also able to learn that the PNIPAm gel shows potential as a drug delivery vehicle. There are however a good number of differences between the system we designed and studied and the one we wish to represent. Among those, the size is of a thousand orders of magnitude different and the printed channel is made of a very stiff and non-sticky material.

Chapter 9

Viscoelastic Slip Coefficient Dependency on Normal Pressure

9.1 Introduction

Through empirical testing we have found that the viscoelastic slip coefficient of polymer gels increases with the normal pressure to which they are subject. A synthesized cylindrical PNIPAm monomer based gel is placed in straight tubes of different radius size to allow for different confinements and, so, normal pressures.

The tube is submerged in water and a difference of pressure is applied through control of the hydraulic head. We measured speed of the gel and the pressure to which the gel is subject, and along with the motion governing equation we derived the viscoelastic slip coefficient μ.

9.2 Shear modulus estimation

Given a cylindrical specimen subject to axial loading, the mapping is given by:

$$\mathfrak{z} = \lambda_Z Z \qquad r = \lambda_R R \tag{9.1}$$

Assume that both λ are constant values. Then the gradient of deformations in axisymmetrical coordinates is given by:

$$F = \begin{pmatrix} \lambda_R & 0 & 0 \\ 0 & \lambda_R & 0 \\ 0 & 0 & \lambda_Z \end{pmatrix} \tag{9.2}$$

Applying conservation of volume $det(F) = 1$ and so $\lambda_R = \frac{1}{\sqrt{\lambda_Z}}$. The strain energy:

$$\psi = \frac{G_{sh}}{2}\left(\lambda_Z^2 + \frac{2}{\lambda_Z} - 3\right) \tag{9.3}$$

And so, the nominal axial force:

$$P_{ZZ} = \frac{\partial \psi}{\partial \lambda_Z} = G_{sh}\left(\lambda_Z - \frac{1}{\lambda_Z^2}\right) \tag{9.4}$$

Figure 9.1: Channel models schematics for 3D printing, straight with ratchet (top), undulating (bottom)

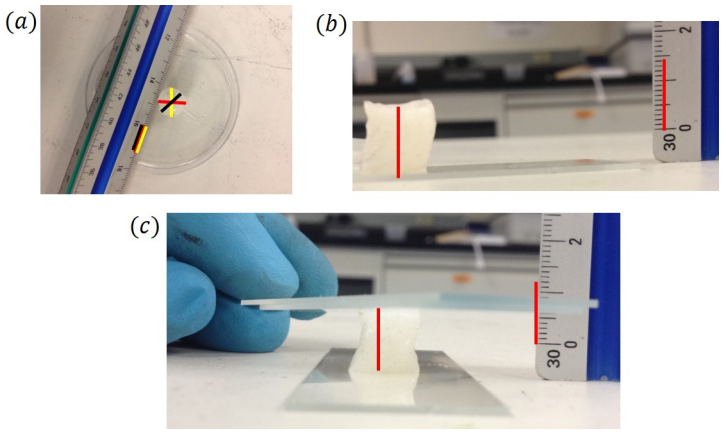

Gel features: 1.2 cm diameter and 1.4 cm length when in rest and when fully swollen. We used glass slides to perform a compression test and measured the deformation. For two glass slides, we found a 14% compression of the body. Applying the hyperelastic equation, we obtained that the shear modulus is $G_{sh} = 1,580 \ \ N/m^2$. Comparing with data on shear modulus for Acrylamide gels [8], ours is very similar given its amount of monomer (8%) and bis-acrylamide (0.1%).

9.3 Slip coefficient - pressure relationship

Applying the hyperelastic model as we did to estimate the shear modulus, the strain energy in terms of λ_R is:

$$\psi = \frac{G_{sh}}{2}\left(2\lambda_R^2 + \frac{1}{\lambda_R^4} - 3\right) \tag{9.5}$$

And so the nominal axial force:

$$P_{RR} = \frac{\partial \psi}{\partial \lambda_R} = 2G_{sh}\left(\lambda_Z - \frac{1}{\lambda_R^5}\right) \tag{9.6}$$

Current area in terms of reference area:

$$A = h2\pi R = \lambda_Z h_0 \pi \lambda_R R_0 = \frac{A_0}{\lambda_R} \tag{9.7}$$

Hence, the confinement pressure:

$$p_c = P_{RR}\frac{A_0}{A} = 2G_{sh}\left(\lambda_R^2 - \frac{1}{\lambda_R^4}\right) \tag{9.8}$$

Nondimensionalizing it, $p_c^* = \frac{p_c}{2G_{sh}}$. Since the gel is confined $\lambda_R = \frac{R_{channel}}{R_{gel,rest}}$. Hence, we can easily derive p_c. To get a practical idea of how confined the gel is, we defined the confinement c, which is directly related to the normal pressure to which the gel is subject.

$$c = \frac{r_{gel} - r_{channel}}{r_{channel}} \tag{9.9}$$

Figure 9.2: Relationship between confinement "c" with confinement pressure p_c for the polymer gel

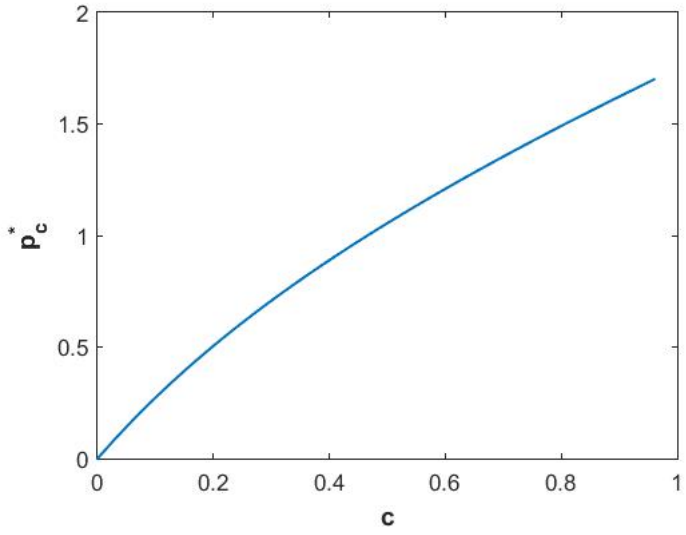

To determine the total normal force applied to the channel walls we simply:

$$N = p_c A = p_c \frac{A_0}{\lambda_R} \tag{9.10}$$

We can estimate the slip coefficient through the motion governing equation:

$$\triangle P = \mu v \tag{9.11}$$

Where $\triangle P$ is the difference in pressure between both sides of the gel that push it forward, v is the velocity the gel achieves and μ the viscoelastic slip coefficient.

Figure 9.3: Slip coefficient pressure dependency empirical results with test results (dots) and minimum least squares fitting (line). Empirical data collection by Anurag Golla.

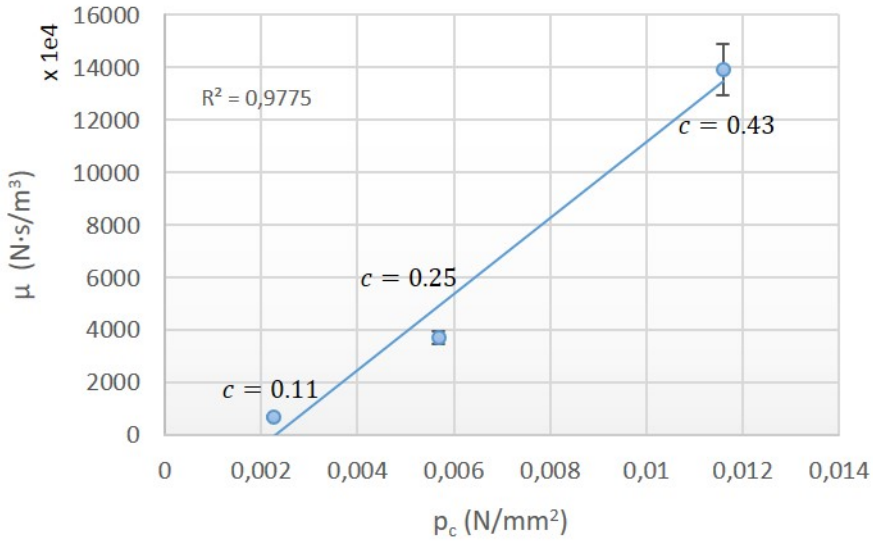

Results clearly show that there is a dependency of μ on the normal pressure to which the gel is subject. Hence, as a gel is subjected to higher confinement, it slips less.

9.4 Viscoelastic friction and slip model

Given the experimental results we can cast the formulation for the friction and slip of polymer gels.

$$F_R \leq \mu_s F_N \Rightarrow v = 0 \tag{9.12}$$

$$F_R > \mu_s F_N \Rightarrow v = \frac{\triangle P}{\mu_v(p_c)} \tag{9.13}$$

Where F_R is the driving force pushing the body to move, μ_s is the static friction coefficient, F_N the normal force, P the confinement pressure and μ_v the viscoelastic slip coefficient (also found as

just μ in this document) which we can write as $\mu_v = \mu_{v,0} + \alpha p_c$.

Figure 9.4: Velocity of gels at different confinements undergoing a difference in pressure empirical results. Empirical data collection by Anurag Golla.

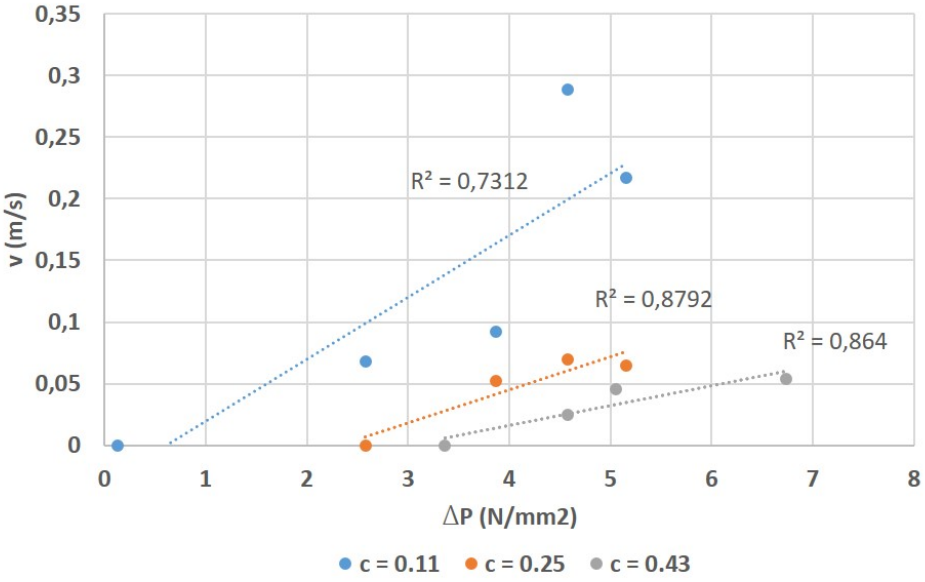

Results show that as gels become more confined it takes a larger difference of pressure for them to move and decreases how the velocities scale with the applied pressure due to the growth of the slip coefficient

9.5 Implementation of a pressure depending slip coefficient to the numerical model

As we have shown, gels show a stick-slip interaction when confined. In our numerical model the driving force that allows the gel to move is not a difference in pressure between both ends of the gel but the frictional forces between wall and membrane, which we defined as:

$$F_{fr} = \frac{\partial \gamma}{\partial \mathfrak{s}} \tag{9.14}$$

For low confinement pressures, the normal force that drives the gel to stick to the channel is not able to avoid the gel from slipping. In our implementation of the channel-membrane in our pressure

depending slip coefficient $\mu(p_c)$, we will consider that the confinement pressures are low enough that the membrane will never be subject to stick conditions. Hence the equation $F_R \leq \mu_s F_N$ will not be implemented.

We can write the $\mu(P_c)$ equation as:

$$\mu(P_c) = \mu_0 + P_c \cdot \alpha \tag{9.15}$$

In the case of straight or conical channels P_c matches with the prescribed difference in pressure between the inside and outside of the membrane. Parameter α is derived from the experimental results and estimated at $15,000 \ \ s/m$. Let us nondimensionalize the equation.

$$\mu^* = \frac{\dot{P}_c R_0^3}{(G_{sh} h_0)^2}\mu \qquad P_c^* = \frac{R_0}{G_{sh} R_0} P_c \tag{9.16}$$

$$\mu^* = \mu_0^* + \alpha^* P_c^* \tag{9.17}$$

Where:

$$\alpha^* = \alpha \frac{\dot{P}_c R_0^2}{G_{sh} h_0} \tag{9.18}$$

After several simulations we have determined that for the range of pressures we are working with in our model, the impact of a confinement pressure depending slip coefficient is very small and so we neglected it.

Bibliography

[1] Kim J. Quillin. "Kinematic Scaling of Locomotion by Hydrostatic Animals: Ontogeny of Peristatic Crawling by the Earthworm Lumbricus Terrestris." The Journal of Experimental Biology 202, 661674 (1999)

[2] Vernerey, Franck J., and Mirmohammadreza Kabiri. "Adaptive Concurrent Multiscale Model for Fracture and Crack Propagation in Heterogeneous Media." Computer Methods in Applied Mechanics and Engineering 276 (2014): 566-88. doi:10.1016/j.cma.2014.03.004.

[3] Nagel, Oliver, Can Guven, Matthias Theves, Meghan Driscoll, Wolfgang Losert, and Carsten Beta. "Geometry-Driven Polarity in Motile Amoeboid Cells." PLoS ONE 9, no. 12 (2014). doi:10.1371/journal.pone.0113382.

[4] Maeda, S., Y. Hara, T. Sakai, R. Yoshida, and S. Hashimoto. "Self-Walking Gel." Adv. Mater. Advanced Materials 19, no. 21 (2007): 3480-484. doi:10.1002/adma.200700625.

[5] Yoshida, Ryo. "Self-Oscillating Gels Driven by the Belousov-Zhabotinsky Reaction as Novel Smart Materials." Adv. Mater. Advanced Materials 22, no. 31 (2010): 3463-483. doi:10.1002/adma.200904075.

[6] Yamada, Munenori, Mizuho Kondo, Ryo Miyasato, Yumiko Naka, Jun-Ichi Mamiya, Motoi Kinoshita, Atsushi Shishido, Yanlei Yu, Christopher J. Barrett, and Tomiki Ikeda. "Photomobile Polymer Materialsvarious Three-dimensional Movements." J. Mater. Chem. 19, no. 1 (2009): 60-62. doi:10.1039/b815289f.

[7] Lämmermann, Tim, and Ronald N. Germain. "The Multiple Faces of Leukocyte Interstitial Migration." Seminars in Immunopathology Semin Immunopathol 36, no. 2 (2014): 227-51. doi:10.1007/s00281-014-0418-8.

[8] Fischer, Robert S., Kenneth A. Myers, Margaret L. Gardel, and Clare M. Waterman. "Stiffness-controlled Three-dimensional Extracellular Matrices for High-resolution Imaging of Cell Behavior." Nat Protoc Nature Protocols 7, no. 11 (2012): 2056-066. doi:10.1038/nprot.2012.127.

[9] Linke, H., B. J. Alemn, L. D. Melling, M. J. Taormina, M. J. Francis, C. C. Dow-Hygelund, V. Narayanan, R. P. Taylor, and A. Stout. "Self-Propelled Leidenfrost Droplets." Phys. Rev. Lett. Physical Review Letters 96, no. 15 (2006). doi:10.1103/physrevlett.96.154502.

[10] Vernerey, Franck J., and Francois Barthelat. "On the Mechanics of Fishscale Structures." International Journal of Solids and Structures 47, no. 17 (2010): 2268-275. doi:10.1016/j.ijsolstr.2010.04.018.

[11] Vernerey, Franck J., and Francois Barthelat. "Skin and Scales of Teleost Fish: Simple Structure but High Performance and Multiple Functions." Journal of the Mechanics and Physics of Solids 68 (2014): 66-76. doi:10.1016/j.jmps.2014.01.005.